LAWRENCE
LIVERMORE
NATIONAL
LABORATORY

LLNL-JRNL-843436

Implicit-Explicit Multirate Infinitesimal Stage-Restart Methods

A. C. Fish, D. R. Reynolds, S. B. Roberts

December 20, 2022

Journal of Computational and Applied Mathematics

Disclaimer

This document was prepared as an account of work sponsored by an agency of the United States government. Neither the United States government nor Lawrence Livermore National Security, LLC, nor any of their employees makes any warranty, expressed or implied, or assumes any legal liability or responsibility for the accuracy, completeness, or usefulness of any information, apparatus, product, or process disclosed, or represents that its use would not infringe privately owned rights. Reference herein to any specific commercial product, process, or service by trade name, trademark, manufacturer, or otherwise does not necessarily constitute or imply its endorsement, recommendation, or favoring by the United States government or Lawrence Livermore National Security, LLC. The views and opinions of authors expressed herein do not necessarily state or reflect those of the United States government or Lawrence Livermore National Security, LLC, and shall not be used for advertising or product endorsement purposes.

Journal of Computational and Applied Mathematics 438 (2024) 115534

Contents lists available at ScienceDirect

Journal of Computational and Applied Mathematics

journal homepage: www.elsevier.com/locate/cam

Implicit–explicit multirate infinitesimal stage-restart methods

Alex C. Fish [a,*,1], Daniel R. Reynolds [a,1], Steven B. Roberts [b,2]

[a] Department of Mathematics, Southern Methodist University, Dallas, TX, USA
[b] Center for Applied Scientific Computing, Lawrence Livermore National Laboratory, Livermore, CA, USA

ARTICLE INFO

Article history:
Received 25 January 2023
Received in revised form 23 August 2023

MSC:
65L05
65L06
65L20

Keywords:
Multirate time integration
Initial-value problems
Implicit–explicit methods

ABSTRACT

Implicit–Explicit (IMEX) methods are flexible numerical time integration methods which solve an initial-value problem (IVP) that is split into stiff and nonstiff processes with the goal of lower computational costs than a purely implicit or explicit approach. A complementary form of flexible IVP solvers are multirate infinitesimal methods for problems split into fast- and slow-changing dynamics, that solve a multirate IVP by evolving a sequence of "fast" IVPs using any suitably accurate algorithm. This article introduces a new class of high-order implicit–explicit multirate methods that are designed for multirate IVPs in which the slow-changing dynamics are further split in an IMEX fashion. This new class, which we call implicit–explicit multirate infinitesimal stage-restart (IMEX-MRI-SR), both improves upon the previous implicit–explicit multirate infinitesimal generalized-structure additive Runge Kutta (IMEX-MRI-GARK) methods by allowing for far easier creation of new embedded methods, and extends multirate exponential Runge Kutta (MERK) methods by allowing the fast-changing dynamics to be nonlinear and the methods to be implicit. We leverage GARK theory to derive conditions for orders of accuracy up to four, and we provide second- and third-order accurate example methods, which are the first known embedded MRI methods with IMEX structure. We then perform numerical simulations demonstrating convergence rates and computational performance in both fixed-step and adaptive-step settings.

© 2023 The Author(s). Published by Elsevier B.V. This is an open access article under the CC BY license (http://creativecommons.org/licenses/by/4.0/).

1. Introduction

Flexible time integration methods for solving systems of initial-value problems (IVPs) have seen growing interest in recent years, largely due to their ability to provide highly accurate approximations of the IVP solution with increased computational efficiency. These integrators strive to reduce computational costs by partitioning the IVP into different components, and then treating each using different step sizes or numerical methods. Some of the primary families of

* Corresponding author.
E-mail addresses: afish@smu.edu (A.C. Fish), reynolds@smu.edu (D.R. Reynolds), roberts115@llnl.gov (S.B. Roberts).

[1] The work of Alex Fish and Daniel Reynolds was supported by the U.S. Department of Energy, Office of Science, Office of Advanced Scientific Computing Research, Scientific Discovery through Advanced Computing (SciDAC) Program through the FASTMath Institute, under DOE award DE-SC0021354.

[2] The work of Steven Roberts was performed under the auspices of the U.S. Department of Energy by Lawrence Livermore National Laboratory under Contract DEAC52-07NA27344 and was supported by the U.S. Department of Energy, Office of Science, Office of Advanced Scientific Computing Research. LLNL-JRNL-843436.

https://doi.org/10.1016/j.cam.2023.115534
0377-0427/© 2023 The Author(s). Published by Elsevier B.V. This is an open access article under the CC BY license (http://creativecommons.org/licenses/by/4.0/).

flexible methods include implicit–explicit (IMEX) partitioning [1–6], linear-nonlinear partitioning [7–11], and multirate partitioning [12–15].

IMEX time integration methods solve IVPs in which the right-hand side function $f(t, y(t))$ is additively split into stiff $\{I\}$ and nonstiff $\{E\}$ processes,

$$\begin{aligned} y'(t) &= f(t,y) := f^{\{I\}}(t,y) + f^{\{E\}}(t,y), \quad t \geq t_0, \\ y(t_0) &= y_0. \end{aligned} \tag{1}$$

IMEX methods then couple two different numerical methods to treat these components: $f^{\{I\}}$ typically uses a stiff but computationally expensive solver, whereas $f^{\{E\}}$ may use a cheaper but nonstiff solver. For example, additive Runge–Kutta (ARK) methods typically combine an A- or L-stable diagonally-implicit Runge–Kutta (DIRK) method with an explicit Runge–Kutta (RK) method.

Similarly, multirate methods solve IVPs in which the right-hand side is additively split into rapidly and slowly evolving dynamics, $\{F\}$ and $\{S\}$,

$$\begin{aligned} y'(t) &= f(t,y) := f^{\{F\}}(t,y) + f^{\{S\}}(t,y), \quad t \geq t_0, \\ y(t_0) &= y_0. \end{aligned} \tag{2}$$

Multirate methods then apply numerical methods with different step sizes for each component to save on computation time while retaining a desired level of accuracy. Because multirate methods evaluate $f^{\{F\}}$ much more frequently than $f^{\{S\}}$, it is assumed to be much cheaper to evaluate.

In this work we combine the above approaches to consider a three-way additively split IVP, wherein the slow partition $f^{\{S\}}$ from (2) is split in an IMEX fashion,

$$\begin{aligned} y'(t) &= f^{\{F\}}(t,y) + f^{\{I\}}(t,y) + f^{\{E\}}(t,y), \quad t \geq t_0, \\ y(t_0) &= y_0. \end{aligned} \tag{3}$$

In particular, we add a new class of methods to the ever-growing family of multirate infinitesimal (MRI) methods. These approximate the solution to (2) or (3) through solving a sequence of "fast" IVPs,

$$\begin{aligned} v_i'(\theta) &= f^{\{F\}}(\theta, v_i) + g_i(\theta), \quad \theta \in [\theta_{0,i}, \theta_{f,i}], \\ v(\theta_{0,i}) &= v_{0,i}. \end{aligned} \tag{4}$$

The forcing functions $g_i(\theta)$ incorporate information from the slow dynamics defined by $f^{\{I\}}$ and $f^{\{E\}}$ in a manner defined by the method to satisfy coupling conditions between fast and slow timescales. In the seminal work on infinitesimal methods, Wensch et al. [15] restricted g_i to constant functions. MRI-GARK methods [13] extended the definition of g_i to include polynomials in time.

MRI methods assume that the fast IVPs (4) are solved exactly, but in practice these are approximated using an additional "fast" numerical method with a smaller step size than the multirate method. An MRI method is agnostic to the choice of fast method, provided it produces sufficiently accurate solutions. This fast method can itself further decompose the problem through IMEX, linear-nonlinear, or multirate approaches.

Our proposed class of methods is called *Implicit-Explicit Multirate Infinitesimal Stage-Restart* (IMEX-MRI-SR) methods. Each stage of an IMEX-MRI-SR method consists of evolving a fast IVP followed by an implicit solve. This allows derivation of IMEX-MRI-SR methods by extending a base ARK method. We discuss the role of base methods further in Section 2.1, particularly focusing on their role in satisfying order conditions. *Stage-Restart* indicates that each stage's fast IVP begins at the initial time step value t_n, in contrast to existing MRI-GARK [13] and IMEX-MRI-GARK [16] methods which begin each stage's fast IVP where the previous stage left off. We discuss the differences between IMEX-MRI-SR methods and MRI-GARK or IMEX-MRI-GARK methods further in Section 1.1.

IMEX-MRI-SR methods are defined by a number of stages $s^{\{S\}}$, n_Ω coefficient matrices $\Omega^{\{k\}} \in \mathbb{R}^{s^{\{S\}} \times s^{\{S\}}}$, $k = 0, \ldots, n_\Omega - 1$, a coefficient matrix $\Gamma \in \mathbb{R}^{s^{\{S\}} \times s^{\{S\}}}$, and an abscissae vector $c^{\{S\}} \in \mathbb{R}^{s^{\{S\}}}$. Embedded versions of these methods include additional coefficient vectors $\hat{\omega}^{\{k\}} \in \mathbb{R}^{s^{\{S\}}}$ and $\hat{\gamma} \in \mathbb{R}^{s^{\{S\}}}$. The algorithm for evolving a solution to an IVP of the form (3) is defined as follows.

Definition 1 (*IMEX-MRI-SR Methods for Additively Split Systems*)**.** An IMEX-MRI-SR method evolves the solution to the problem (3) from t_n to $t_n + H$ according to the following algorithm.

Let: $Y_1^{\{S\}} := y_n$ (5a)

For: $i = 2, \ldots, s^{\{S\}}$

$$\begin{cases} \text{Let:} & v_i(0) \coloneqq y_n, \\ \text{Solve:} & v_i'(\theta) = f^{\{F\}}(t_n+\theta, v_i(\theta)) + g_i(\theta), \ \text{for } \theta \in [0, c_i^{\{S\}}H] \\ & \text{where } g_i(\theta) = \dfrac{1}{c_i^{\{S\}}} \displaystyle\sum_{j=1}^{i-1} \omega_{i,j}\left(\dfrac{\theta}{c_i^{\{S\}}H}\right)\left(f_j^{\{E\}} + f_j^{\{I\}}\right) \\ \text{Solve:} & Y_i^{\{S\}} = v_i\left(c_i^{\{S\}}H\right) + H\displaystyle\sum_{j=1}^{i} \gamma_{i,j} f_j^{\{I\}}, \end{cases} \tag{5b}$$

$$\text{Let: } y_{n+1} \coloneqq Y_{s^{\{S\}}}^{\{S\}}, \tag{5c}$$

$$\begin{cases} \text{Let:} & \hat{v}(0) \coloneqq y_n, \\ \text{Solve:} & \hat{v}(\theta) = f^{\{F\}}(t_n+\theta, \hat{v}(\theta)) + \hat{g}(\theta), \ \text{for } \theta \in [0, H] \\ & \text{where } \hat{g}(\theta) = \displaystyle\sum_{j=1}^{s^{\{S\}}-1} \hat{\omega}_j\left(\dfrac{\theta}{H}\right)\left(f_j^{\{E\}} + f_j^{\{I\}}\right) \\ \text{Solve:} & \hat{y}_{n+1} = \hat{v}(H) + H\displaystyle\sum_{j=1}^{s^{\{S\}}-1} \hat{\gamma}_j f_j^{\{I\}} + H\hat{\gamma}_{s^{\{S\}}} f^{\{I\}}(t_n+H, \hat{y}_{n+1}), \end{cases} \tag{5d}$$

where $f_j^{\{E\}} \coloneqq f^{\{E\}}\left(t_n + c_j^{\{S\}}H, Y_j^{\{S\}}\right)$ and $f_j^{\{I\}} \coloneqq f^{\{I\}}\left(t_n + c_j^{\{S\}}H, Y_j^{\{S\}}\right)$. Here y_{n+1} is the time-evolved approximation to $y(t_n+H)$, and $\hat{y}_{n+1}$ is an embedded solution used for temporal error estimation. It is embedded in the sense that it shares and reuses the function evaluations $f_j^{\{E\}}$ and $f_j^{\{I\}}$ with the primary solution. The embedding does not share evaluations of $f^{\{F\}}$, however, due to the slightly different trajectories of $v(\theta)$ and $\hat{v}(\theta)$. If temporal error estimation is not needed, then step (5d) may be omitted.

Definition 2 (*Slow Tendency Coefficients*)**.** The coefficients $\omega_{i,j}$ in (5b) are defined as in [16]

$$\omega_{i,j}(\tau) \coloneqq \sum_{k=0}^{n_\Omega-1} \omega_{i,j}^{\{k\}}\tau^k, \quad \overline{\omega}_{i,j} \coloneqq \int_0^1 \omega_{i,j}(\tau)\mathrm{d}\tau = \sum_{k=0}^{n_\Omega-1} \frac{\omega_{i,j}^{\{k\}}}{k+1}, \tag{6}$$

and the embedding functions $\hat{\omega}_j(\tau)$ are defined similarly, with vectors of coefficients $\hat{\omega}^{\{k\}}$. We group the coefficients coefficients $\{\omega_{i,j}^{\{k\}}\}$, $\{\overline{\omega}_{i,j}\}$, and $\{\gamma_{i,j}\}$ into the $s^{\{S\}}\times s^{\{S\}}$ matrices $\Omega^{\{k\}}$, $\overline{\Omega}$, and Γ, respectively. As in [16] we assume that $\Omega^{\{k\}}$ and $\overline{\Omega}$ are strictly lower-triangular. We note that $\overline{\Omega}$ is not used in defining the method above, however it arises in the ensuing order conditions in Section 2. As with the number of stages, larger values of n_Ω add more available coefficients which can then be used to satisfy additional order conditions while simultaneously increasing the computational effort, so a balance must be struck when deriving new methods.

The rest of this paper is structured as follows. In the next subsection, we present related methods to IMEX-MRI-SR, discussing both their similarities and their limitations that are improved upon by the proposed methods. In Section 2 we prove order conditions for IMEX-MRI-SR methods up to order four, and in Section 3 we analyze the linear stability of this class of methods. In Section 4 we provide embedded IMEX-MRI-SR methods of orders 2 and 3. In Section 5 we show that a previous class of multirate methods may be reformulated as IMEX-MRI-SR methods, and we use our convergence theory to show previously unproven features of those methods. We then present numerical results in Section 6 to validate our convergence theory, and to compare the efficiency of IMEX-MRI-SR methods against existing methods for problems of the form (3). Finally, in Section 7 we conclude this article, summarizing our contributions and discussing future work.

1.1. Related methods

To our knowledge, there exist two primary mechanisms for allowing both IMEX partitioning of the slow dynamics and infinitesimal treatment of the fast dynamics. The first consists of standard operator-splitting methods, including the first-order accurate "Lie–Trotter" [17,18] and the second-order accurate "Strang–Marchuk" [19,20] schemes. The second mechanism comes from the recent up to fourth-order IMEX-MRI-GARK [16] methods, an IMEX variation of MRI-GARK [13] methods. The Lie–Trotter and Strang–Marchuk methods, as well as more recent "fractional step" methods [21] operate by sequentially applying distinct solvers to each component, only communicating with one another through the initial conditions applied within each sub-solve. Variations of both Lie–Trotter and Strang–Marchuk methods for the IMEX multirate splitting (3) are shown in [16]. However, Lie–Trotter and Strang–Marchuk are limited to at most first and second order accuracy in time, regardless of the order of accuracy of each component solver. Furthermore, to achieve higher order than two, fractional step methods must include integration in the reverse time direction [22], which can be impractical in some applications. As the definition of these splitting methods rely upon component solvers and the order in which they are applied, we describe a concrete definition used in our numerical experiments in Section 6.1.

IMEX-MRI-GARK methods are organized similarly to IMEX-MRI-SR, in that they advance the solution by alternating between evolving fast IVPs and solving implicit algebraic equations involving $f^{\{I\}}$, and they use the result from each stage to provide a contribution to $g_i(\theta)$ for later stages. However, unlike IMEX-MRI-SR methods, IMEX-MRI-GARK methods evolve each fast IVP over an interval $[c_{i-1}H, c_iH]$, with an initial condition given as the result of the previous stage. In each stage, either a fast evolution or implicit solve may occur, with this choice dictated by the abscissae: when $\Delta c_i := c_i - c_{i-1} > 0$ a fast evolution occurs, but when $\Delta c_i = 0$ an algebraic system must be solved. In all existing implicit MRI-GARK and IMEX-MRI-GARK methods, authors have derived schemes by beginning with a base DIRK or ARK method, and then introduced additional internal stages to ensure an alternating pattern of $\Delta c_i \neq 0$ followed by $\Delta c_{i+1} = 0$, thereby ensuring an appropriate structure [13,16]. However, these methods inherently require abscissae vectors $c^{\{S\}}$ that are non-decreasing. This is generally an uncommon feature in RK methods, especially for orders of accuracy higher than two [4–6,23–26], so there are relatively few base DIRK and ARK methods available for deriving new MRI-GARK and IMEX-MRI-GARK methods. Additionally, the "padding" process for adding internal stages to a DIRK or ARK method to ensure $\Delta c_i = 0$ adds significant complexity. As a result of these challenges, no authors have successfully created IMEX-MRI-GARK methods with embeddings for temporal error estimation.

A second class of methods that are closely related to IMEX-MRI-SR are multirate exponential Runge–Kutta (MERK) methods [8]. While these do not support implicitness at the slow time scale (i.e., $f^{\{I\}} = 0$), and they assume that the fast function is linear (i.e., $f^{\{F\}}(t, y) = \mathcal{L}y$), their structure matches (5). Each internal stage is computed through evolving a fast IVP over an interval $[0, c_iH]$, using a forcing function that is determined using values of $f^{\{E\}}$ at previous slow stages.

2. IMEX-MRI-SR order conditions

Similar to IMEX-MRI-GARK methods, we derive order conditions for IMEX-MRI-SR methods by first representing the algorithm in GARK form. Due to the 3-component splitting (3), we must identify GARK coefficients $\mathbf{A}^{\{\sigma,\nu\}}$, $\mathbf{b}^{\{\nu\}}$, and $\mathbf{c}^{\{\nu\}}$ for $\sigma \in \{S, F\}$ and $\nu \in \{I, E, F\}$. We reserve boldface for these GARK coefficients and refer to $\mathbf{A}^{\{F,\nu\}}$, $\nu \in \{I, E, F\}$ as the fast GARK tables, and to $\mathbf{A}^{\{S,\nu\}}$, $\nu \in \{I, E, F\}$ as the slow GARK tables. Our analysis in this section relies on the following set of assumptions.

Assumption 1. We assume the fast IVP (5b) is solved with one step of a sufficiently accurate Runge–Kutta method referred to as the "fast method", having $s^{\{F\}}$ stages, and defined by the Butcher table $(A^{\{F\}}, b^{\{F\}}, c^{\{F\}})$.

Assumption 2. First-order IMEX-MRI-SR methods assume the fast method from Assumption 1 is at least order $\max(1, n_\Omega)$ accurate.

Assumption 3. Second-order IMEX-MRI-SR methods assume the fast method from Assumption 1 is at least order $\max(2, n_\Omega)$ accurate.

Assumption 4. Third-order IMEX-MRI-SR methods assume the fast method from Assumption 1 is at least order $\max(3, n_\Omega + 1)$ accurate.

Assumption 5. Fourth-order IMEX-MRI-SR methods assume the fast method from Assumption 1 is at least order $\max(4, n_\Omega + 2)$ accurate.

The jth sub-stage in computing the solution to the fast IVP $v_i'(\theta)$ is given by

$$V_{i,j} = y_n + c_i^{\{S\}} H \sum_{k=1}^{s^{\{F\}}} a_{j,k}^{\{F\}} f_{i,k}^{\{F\}} + H \sum_{k=1}^{s^{\{F\}}} a_{j,k}^{\{F\}} \sum_{\ell=1}^{i-1} \omega_{i,\ell}(c_k^{\{F\}}) \left(f_\ell^{\{E\}} + f_\ell^{\{I\}} \right) \tag{7}$$

for $i = 1, \ldots, s^{\{S\}}$, and $j = 1, \ldots, s^{\{F\}}$, where $f_{i,k}^{\{F\}} := f^{\{F\}}(t_n + c_k^{\{F\}} H, V_{i,k})$, $f_\ell^{\{E\}} := f^{\{E\}}(t_n + c_\ell^{\{S\}} H, Y_\ell^{\{S\}})$ and $f_\ell^{\{I\}} := f^{\{I\}}(t_n + c_\ell^{\{S\}} H, Y_\ell^{\{S\}})$. The IMEX-MRI-SR method's slow stages $Y_i^{\{S\}}$, $i = 1, \ldots, s^{\{S\}}$, are then computed by

$$\begin{aligned} Y_i^{\{S\}} = y_n &+ c_i^{\{S\}} H \sum_{j=1}^{s^{\{F\}}} b_j^{\{F\}} f_{i,j}^{\{F\}} \\ &+ H \sum_{j=1}^{s^{\{F\}}} b_j^{\{F\}} \sum_{\ell=1}^{i-1} \omega_{i,\ell}\left(c_j^{\{F\}}\right) \left(f_\ell^{\{E\}} + f_\ell^{\{I\}} \right) + H \sum_{\ell=1}^{i} \gamma_{i,\ell} f_\ell^{\{I\}}. \end{aligned} \tag{8}$$

We leverage GARK theory [6] to construct order conditions as in [13,16]. Since the slow partitions share the same stages, $Y_i^{\{S\}}$, these methods have six GARK matrices, $\mathbf{A}^{\{F,F\}}$, $\mathbf{A}^{\{F,E\}}$, $\mathbf{A}^{\{F,I\}}$, $\mathbf{A}^{\{S,F\}}$, $\mathbf{A}^{\{S,E\}}$, and $\mathbf{A}^{\{S,I\}}$ and three GARK vectors $\mathbf{b}^{\{F\}}$,

$\mathbf{b}^{\{E\}}$, and $\mathbf{b}^{\{I\}}$,

$$\begin{array}{c|c|c} \mathbf{A}^{\{F,F\}} & \mathbf{A}^{\{F,E\}} & \mathbf{A}^{\{F,I\}} \\ \hline \mathbf{A}^{\{S,F\}} & \mathbf{A}^{\{S,E\}} & \mathbf{A}^{\{S,I\}} \\ \hline \left(\mathbf{b}^{\{F\}}\right)^T & \left(\mathbf{b}^{\{E\}}\right)^T & \left(\mathbf{b}^{\{I\}}\right)^T \end{array}.$$

Here, $\mathbf{A}^{\{F,F\}}$ is a square $s^{\{SF\}} \times s^{\{SF\}}$ matrix (where we define $s^{\{SF\}} = s^{\{S\}} \cdot s^{\{F\}}$), containing the coefficients relating the fast stages $\{V_{i,j}\}$ to each other. It is block-diagonal because $V_{i,j}$ depends only on $V_{i,k}$, $k = 1, \ldots, s^{\{F\}}$ through the $A^{\{F\}}$ coefficients, and never on $V_{\ell,j}$, $\ell \neq i$. We name these $s^{\{F\}} \times s^{\{F\}}$ block-diagonal elements as $A^{\{F,F,i\}}$.

$\mathbf{A}^{\{F,E\}}$ and $\mathbf{A}^{\{F,I\}}$ are tall $s^{\{SF\}} \times s^{\{S\}}$ matrices relating the fast stages $\{V_{i,j}\}$ to the explicit and implicit function evaluations of the slow stages $\{Y_i^{\{S\}}\}$. We name the $s^{\{S\}}$ blocks that comprise each of these as $A^{\{F,E,i\}}$ and $A^{\{F,I,i\}}$, respectively.

$\mathbf{A}^{\{S,F\}}$ is a wide $s^{\{S\}} \times s^{\{SF\}}$ matrix, containing the coefficients relating the slow stages $\{Y_i^{\{S\}}\}$ to the fast stages $\{V_{i,j}\}$. We name these $s^{\{S\}}$ total $s^{\{S\}} \times s^{\{F\}}$ blocks that comprise $\mathbf{A}^{\{S,F\}}$ as $A^{\{S,F,i\}}$. Each $A^{\{S,F,i\}}$ contains at most one row of non-zero entries, located in row i, because $Y_i^{\{S\}}$ depends only on $V_{i,j}$, $j = 1, \ldots, s^{\{F\}}$, and never on $V_{\ell,j}$, $\ell \neq i$.

$\mathbf{A}^{\{S,E\}}$ and $\mathbf{A}^{\{S,I\}}$ are square $s^{\{S\}} \times s^{\{S\}}$ matrices relating the slow stages $\{Y_i^{\{S\}}\}$ to the explicit and implicit function evaluations of those slow stages.

The vectors $\mathbf{b}^{\{\sigma\}}$ equal the last rows of $\mathbf{A}^{\{S,\sigma\}}$, $\sigma \in \{F, E, I\}$, so that the GARK matrices match IMEX-MRI-SR methods in having the first-same-as-last (FSAL) property, where the last stage is used as the solution to the step.

When an embedding (5d) is included, it will correspond to three additional GARK vectors, $\hat{\mathbf{b}}^{\{F\}}$ $\hat{\mathbf{b}}^{\{E\}}$ and $\hat{\mathbf{b}}^{\{I\}}$. Due to the structural similarity of (5d) to the last stage $Y_{s^{\{S\}}}^{\{S\}}$, the contents of these vectors will only differ from $\mathbf{b}^{\{F\}}$, $\mathbf{b}^{\{E\}}$ and $\mathbf{b}^{\{I\}}$ through their dependence on $\hat{\omega}_j^{\{k\}}$ and $\hat{\gamma}_j$ instead of $\omega_{s^{\{S\}},j}^{\{k\}}$ and $\gamma_{s^{\{S\}},j}$. Thus the order conditions that follow for the primary GARK matrices and vectors can be applied to the embedding as well.

With the above simplifications, the GARK tableau can be expressed in block-matrix form as

$$\begin{array}{ccc|c|c} A^{\{F,F,1\}} & & & A^{\{F,E,1\}} & A^{\{F,I,1\}} \\ & \ddots & & \vdots & \vdots \\ & & A^{\{F,F,s^{\{S\}}\}} & A^{\{F,E,s^{\{S\}}\}} & A^{\{F,I,s^{\{S\}}\}} \\ \hline A^{\{S,F,1\}} & \cdots & A^{\{S,F,s^{\{S\}}\}} & \mathbf{A}^{\{S,E\}} & \mathbf{A}^{\{S,I\}} \\ \hline \multicolumn{3}{c|}{\left(\mathbf{b}^{\{F\}}\right)^T} & \left(\mathbf{b}^{\{E\}}\right)^T & \left(\mathbf{b}^{\{I\}}\right)^T \end{array}.$$

A GARK method with this tabular structure has stage update formulas

$$V_{i,j} = y_n + H \sum_{k=1}^{s^{\{F\}}} a_{j,k}^{\{F,F,i\}} f_{i,j}^{\{F\}} + H \sum_{k=1}^{s^{\{F\}}} a_{j,k}^{\{F,E,i\}} f_j^{\{E\}} + H \sum_{k=1}^{s^{\{F\}}} a_{j,k}^{\{F,I,i\}} f_j^{\{I\}}, \tag{9a}$$

$$Y_i^{\{S\}} = y_n + H \sum_{j=1}^{s^{\{F\}}} a_{i,j}^{\{S,F,i\}} f_{ij}^{\{F\}} + H \sum_{j=1}^{s^{\{F\}}} \mathbf{A}_{i,j}^{\{S,E\}} f_j^{\{E\}} + H \sum_{j=1}^{s^{\{F\}}} \mathbf{A}_{i,j}^{\{S,I\}} f_j^{\{I\}}. \tag{9b}$$

By matching coefficients in (7) and (9a), we identify the fast GARK coefficients,

$$a_{j,k}^{\{F,F,i\}} = c_i^{\{S\}} a_{j,k}^{\{F\}}, \tag{10a}$$

$$a_{j,\ell}^{\{F,E,i\}} = \sum_{l=1}^{s^{\{F\}}} a_{j,k}^{\{F\}} \omega_{i,\ell}(c_l^{\{F\}}) = \sum_{l=1}^{s^{\{F\}}} \sum_{k=0}^{n_\Omega - 1} \omega_{i,\ell}^{\{k\}} a_{j,l}^{\{F\}} \left(c_l^{\{F\}}\right)^k, \tag{10b}$$

$$a_{j,\ell}^{\{F,I,i\}} = a_{j,\ell}^{\{F,E,i\}} = \sum_{k=1}^{s^{\{F\}}} b_{j,k}^{\{F\}} \omega_{i,\ell}(c_k^{\{F\}}), \tag{10c}$$

Converting these to matrix form, we have the fast GARK tables,

$$\mathbf{A}^{\{F,F\}} = C^{\{S\}} \otimes A^{\{F\}} \in \mathbb{R}^{s^{\{SF\}} \times s^{\{SF\}}}, \tag{11a}$$

$$\mathbf{A}^{\{F,E\}} = \sum_{k=0}^{n_\Omega - 1} \Omega^{\{k\}} \otimes A^{\{F\}} \left(c^{\{F\}}\right)^k \in \mathbb{R}^{s^{\{SF\}} \times s^{\{S\}}}, \tag{11b}$$

$$\mathbf{A}^{\{F,I\}} = \mathbf{A}^{\{F,E\}} = \sum_{k=0}^{n_\Omega - 1} \Omega^{\{k\}} \otimes A^{\{F\}} \left(c^{\{F\}}\right)^k \in \mathbb{R}^{s^{\{SF\}} \times s^{\{S\}}}, \tag{11c}$$

where $\otimes$ denotes the Kronecker product, exponentiation of vectors is performed component-wise, and $C^{\{\sigma\}} = \text{diag}(c^{\{\sigma\}})$.

We similarly find the slow GARK table coefficients by comparing (8) and (9b),

$$a_{i,j}^{\{S,F,i\}} = c_i^{\{S\}} b_j^{\{F\}}, \tag{12a}$$

$$a_{i,\ell}^{\{S,E\}} = \sum_{k=1}^{s^{\{F\}}} b_k^{\{F\}} \omega_{i,\ell}(c_k^{\{F\}}) = \sum_{k=0}^{n_\Omega - 1} \omega_{i,\ell}^{\{k\}} \left(b^{\{F\}}\right)^T \left(c^{\{F\}}\right)^k, \tag{12b}$$

$$a_{i,\ell}^{\{S,I\}} = \sum_{k=1}^{s^{\{F\}}} b_k^{\{F\}} \omega_{i,\ell}\left(c_j^{\{F\}}\right) + \gamma_{i,\ell} = \sum_{k=0}^{n_\Omega - 1} \omega_{i,\ell}^{\{k\}} \left(b^{\{F\}}\right)^T \left(c^{\{F\}}\right)^k + \gamma_{i,\ell}. \tag{12c}$$

Assumptions 2 through 5 are sufficient to guarantee that

$$\left(b^{\{F\}}\right)^T \left(c^{\{F\}}\right)^k = \frac{1}{k+1}, \quad k = 0, \ldots, n_\Omega - 1.$$

Leveraging this, and examining (12), the slow GARK tables in matrix-form are

$$\mathbf{A}^{\{S,F\}} = C^{\{S\}} \otimes \left(b^{\{F\}}\right)^T \in \mathbb{R}^{s^{\{S\}} \times s^{\{SF\}}}, \tag{13a}$$

$$\mathbf{A}^{\{S,E\}} = \sum_{k=0}^{n_\Omega - 1} \Omega^{\{k\}} \frac{1}{k+1} = \overline{\Omega} \in \mathbb{R}^{s^{\{S\}} \times s^{\{S\}}}, \tag{13b}$$

$$\mathbf{A}^{\{S,I\}} = \sum_{k=0}^{n_\Omega - 1} \Omega^{\{k\}} \frac{1}{k+1} + \Gamma = \overline{\Omega} + \Gamma \in \mathbb{R}^{s^{\{S\}} \times s^{\{S\}}}. \tag{13c}$$

Leveraging the fact that IMEX-MRI-SR methods have the FSAL property with respect to the slow stages $Y^{\{S\}}$, we identify the remaining GARK coefficients,

$$\left(\mathbf{b}^{\{F\}}\right)^T = e_{s^{\{S\}}}^T \mathbf{A}^{\{S,F\}} = C^{\{S\}} e_{s^{\{S\}}} \otimes \left(b^{\{F\}}\right)^T = (e_{s^{\{S\}}} \otimes b^{\{F\}})^T, \tag{14a}$$

$$\left(\mathbf{b}^{\{E\}}\right)^T = e_{s^{\{S\}}}^T \mathbf{A}^{\{S,E\}} = e_{s^{\{S\}}}^T \overline{\Omega}, \tag{14b}$$

$$\left(\mathbf{b}^{\{I\}}\right)^T = e_{s^{\{S\}}}^T \mathbf{A}^{\{S,I\}} = e_{s^{\{S\}}}^T (\overline{\Omega} + \Gamma), \tag{14c}$$

where $e_{s^{\{S\}}}$ is an $s^{\{S\}}$-length vector of all zeroes except a one in the last position.

2.1. Base consistency

If $f^{\{F\}}(t, y) = 0$, then an IMEX-MRI-SR method reduces to a simple ARK method defined by slow explicit and implicit base methods,

$$(A^{\{E\}}, b^{\{E\}}, c^{\{E\}}) = (\mathbf{A}^{\{S,E\}}, \mathbf{b}^{\{E\}}, \mathbf{A}^{\{S,E\}} \mathbb{1}^{s^{\{S\}}}),$$
$$(A^{\{I\}}, b^{\{I\}}, c^{\{I\}}) = (\mathbf{A}^{\{S,I\}}, \mathbf{b}^{\{I\}}, \mathbf{A}^{\{S,I\}} \mathbb{1}^{s^{\{S\}}}),$$

where $\mathbb{1}^{s^{\{S\}}}$ is a vector of ones with length $s^{\{S\}}$. We will refer to this ARK method as the slow base method throughout the derivation of the order conditions.

Remark 1 (*First Order Conditions*)**.** As long as the slow base method is first-order accurate and the fast method satisfies Assumption 2, there are no additional first-order coupling conditions for a GARK method. Thus, the effective first-order IMEX-MRI-SR condition is that $\mathbf{A}^{\{S,E\}} = \overline{\Omega}$ and $\mathbf{A}^{\{S,I\}} = \overline{\Omega} + \Gamma$ form an order one ARK method, which can be simply achieved if both $\mathbf{A}^{\{S,E\}}$ and $\mathbf{A}^{\{S,I\}}$ have first-order accuracy.

Remark 2 (*Deriving IMEX-MRI-SR Methods from Existing ARK Methods*)**.** Due to the IMEX-MRI-SR structure, a base ARK method should be stiffly-accurate; otherwise it must first be converted to stiffly-accurate form by appending the b vectors to the bottom and pad a column of zeros to the right of the ARK's A matrices.

2.2. Kronecker product identities

In the ensuing derivations we leverage the following identities:

$$(A \otimes B)^T = A^T \otimes B^T, \tag{15a}$$

$$(A \otimes B)(C \otimes D) = (AC) \otimes (BD), \tag{15b}$$

$$(A \otimes v)\mathbb{1}^{\{r(A)\}} = (A\mathbb{1}^{\{r(A)\}}) \otimes v, \tag{15c}$$
$$(v \otimes A)\mathbb{1}^{\{r(A)\}} = v \otimes (A\mathbb{1}^{\{r(A)\}}), \tag{15d}$$

where A, B, C, D are arbitrary matrices with compatible dimensions, v is an arbitrary vector, and $\mathbb{1}^{\{r(A)\}}$ is a vector of ones with length equal to the number of rows of A. Identities (15a) and (15b) can be found in [27]. Identities (15c) and (15d) can be shown through elementary computation.

2.3. GARK internal consistency

Theorem 1 (*GARK Internal Consistency*)**.** *An IMEX-MRI-SR method satisfies the GARK internal consistency conditions,*

$$\mathbf{c}^{\{F,F\}} = \mathbf{c}^{\{F,E\}} = \mathbf{c}^{\{F,I\}}, \tag{16a}$$
$$\mathbf{c}^{\{S,F\}} = \mathbf{c}^{\{S,E\}} = \mathbf{c}^{\{S,I\}}, \tag{16b}$$

where $\mathbf{c}^{\{F,\nu\}} = \mathbf{A}^{\{F,\nu\}}\mathbb{1}^{s^{\{\nu\}}}$, $\mathbf{c}^{\{S,\nu\}} = \mathbf{A}^{\{S,\nu\}}\mathbb{1}^{s^{\{\nu\}}}$, $\nu \in \{I, E, F\}$, *if the following conditions hold:*

$$\Omega^{\{0\}}\mathbb{1}^{s^{\{S\}}} = c^{\{S\}}, \tag{17a}$$
$$\Omega^{\{k\}}\mathbb{1}^{s^{\{S\}}} = 0^{s^{\{S\}}}, \ k = 1, \ldots, n_\Omega - 1, \tag{17b}$$
$$\Gamma\mathbb{1}^{s^{\{S\}}} = 0^{s^{\{S\}}}, \tag{17c}$$

where $0^{s^{\{S\}}}$ *is a vector of zeros with length* $s^{\{S\}}$.

Proof. Computing the fast GARK abscissae from the respective GARK tables,

$$\begin{aligned}
\mathbf{c}^{\{F,F\}} &= \mathbf{A}^{\{F,F\}}\mathbb{1}^{s^{\{SF\}}} = (C^{\{S\}} \otimes A^{\{F\}})\mathbb{1}^{s^{\{SF\}}} = c^{\{S\}} \otimes c^{\{F\}}, \\
\mathbf{c}^{\{F,E\}} &= \mathbf{A}^{\{F,E\}}\mathbb{1}^{s^{\{S\}}} = \sum_{k=0}^{n_\Omega - 1} \left(\Omega^{\{k\}} \otimes A^{\{F\}}\left(c^{\{F\}}\right)^k\right)\mathbb{1}^{s^{\{S\}}} \\
&= (\Omega^{\{0\}}\mathbb{1}^{s^{\{S\}}}) \otimes c^{\{F\}} + \sum_{k=1}^{n_\Omega - 1} (\Omega^{\{k\}}\mathbb{1}^{s^{\{S\}}}) \otimes A^{\{F\}}\left(c^{\{F\}}\right)^k, \\
\mathbf{c}^{\{F,I\}} &= \mathbf{A}^{\{F,I\}}\mathbb{1}^{s^{\{S\}}} = \mathbf{A}^{\{F,E\}}\mathbb{1}^{s^{\{S\}}} = \mathbf{c}^{\{F,E\}},
\end{aligned}$$

thus $\mathbf{c}^{\{F,F\}} = \mathbf{c}^{\{F,I\}} = \mathbf{c}^{\{F,E\}}$ when $\Omega^0\mathbb{1}^{s^{\{S\}}} = c^{\{S\}}$ and $\Omega^{\{k\}}\mathbb{1}^{s^{\{S\}}} = 0^{s^{\{S\}}}$, $k = 1, \ldots, n_\Omega - 1$. Computing the slow GARK abscissae from the slow GARK tables,

$$\begin{aligned}
\mathbf{c}^{\{S,F\}} &= \mathbf{A}^{\{S,F\}}\mathbb{1}^{s^{\{SF\}}} = (C^{\{S\}} \otimes b^{\{F\}})\mathbb{1}^{s^{\{SF\}}} = c^{\{S\}}, \\
\mathbf{c}^{\{S,E\}} &= \mathbf{A}^{\{S,E\}}\mathbb{1}^{s^{\{S\}}} = \overline{\Omega}\mathbb{1}^{s^{\{S\}}} = \sum_{k=0}^{n_\Omega - 1} \Omega^{\{k\}}\mathbb{1}^{s^{\{S\}}}\frac{1}{k+1}, \\
\mathbf{c}^{\{S,E\}} &= \mathbf{A}^{\{S,I\}}\mathbb{1}^{s^{\{S\}}} = (\overline{\Omega} + \Gamma)\mathbb{1}^{s^{\{S\}}} = \sum_{k=0}^{n_\Omega - 1} \Omega^{\{k\}}\mathbb{1}^{s^{\{S\}}}\frac{1}{k+1} + \Gamma\mathbb{1}^{s^{\{S\}}},
\end{aligned}$$

and thus $\mathbf{c}^{\{S,F\}} = \mathbf{c}^{\{S,I\}} = \mathbf{c}^{\{S,E\}}$ is satisfied using the same conditions as above, with the additional constraint that $\Gamma\mathbb{1}^{s^{\{S\}}} = 0^{s^{\{S\}}}$.

Remark 3 (*Second Order Conditions*)**.** When the tables that comprise a GARK method are each at least second-order accurate and internal consistency holds, there are no additional second-order coupling conditions. Thus, the internal consistency conditions act as second-order conditions when the slow base method is second-order accurate and the fast method satisfies Assumption 3.

2.4. Higher order conditions

Theorem 2 (*Third Order Conditions*)**.** *An internally-consistent IMEX-MRI-SR method with third-order accurate slow base method and with fast method satisfying Assumption 4 is third-order accurate if the following condition holds:*

$$e_{s^{\{S\}}}^T\left(\sum_{k=0}^{n_\Omega - 1} \Omega^{\{k\}}\frac{1}{(k+1)(k+2)}\right)c^{\{S\}} = \frac{1}{6}. \tag{18}$$

Proof. From [16], an internally consistent GARK method of this structure with a third-order accurate slow base method and an order $\max(3, n_\Omega + 1)$ fast method has four third-order coupling conditions,

$$\left(\mathbf{b}^{\{\sigma\}}\right)^T \mathbf{A}^{\{S,F\}}\mathbf{c}^{\{F\}} = \frac{1}{6}, \tag{19a}$$

$$\left(\mathbf{b}^{\{F\}}\right)^T \mathbf{A}^{\{S,\sigma\}}\mathbf{c}^{\{S\}} = \frac{1}{6}, \tag{19b}$$

for $\sigma \in \{I, E\}$. An internally-consistent IMEX-MRI-SR method has

$$\mathbf{c}^{\{F\}} = \mathbf{c}^{\{F,F\}} = \mathbf{c}^{\{F,E\}} = \mathbf{c}^{\{F,I\}} = c^{\{S\}} \otimes c^{\{F\}}, \tag{20a}$$

$$\mathbf{c}^{\{S\}} = \mathbf{c}^{\{S,F\}} = \mathbf{c}^{\{S,E\}} = \mathbf{c}^{\{S,I\}} = c^{\{E\}} = c^{\{I\}} = c^{\{S\}}. \tag{20b}$$

Conditions (19a) are automatically satisfied for both values of σ:

$$\begin{aligned}\frac{1}{6} &= \left(\mathbf{b}^{\{\sigma\}}\right)^T \mathbf{A}^{\{S,F\}}\mathbf{c}^{\{F\}} \\ &= \left(b^{\{\sigma\}}\right)^T \left(C^{\{S\}} \otimes \left(b^{\{F\}}\right)^T\right)\left(c^{\{S\}} \otimes c^{\{F\}}\right) = \frac{1}{3}\cdot\frac{1}{2}.\end{aligned}$$

Conditions (19b) reduce to the single condition (18) because $\mathbf{A}^{\{F,E\}} = \mathbf{A}^{\{F,I\}}$ for an IMEX-MRI-SR method:

$$\begin{aligned}\frac{1}{6} &= \left(\mathbf{b}^{\{F\}}\right)^T \mathbf{A}^{\{F,\sigma\}}\mathbf{c}^{\{S\}} = \left(e_{s^{\{S\}}} \otimes b^{\{F\}}\right)^T \left(\sum_{k=0}^{n_\Omega-1} \Omega^{\{k\}} \otimes A^{\{F\}}\left(c^{\{F\}}\right)^k\right) c^{\{S\}} \\ &= e_{s^{\{S\}}}^T \left(\sum_{k=0}^{n_\Omega-1} \Omega^{\{k\}} \frac{1}{(k+1)(k+2)}\right) c^{\{S\}}.\end{aligned}$$

Theorem 3 (*Fourth Order Conditions*)**.** *An IMEX-MRI-SR method satisfying Theorem 2 is fourth-order accurate if the slow base method is fourth-order accurate, the fast method satisfies Assumption 5, and the following conditions hold:*

$$e_{s^{\{S\}}}^T \left(\sum_{k=0}^{n_\Omega-1} \Omega^{\{k\}} \frac{1}{(k+1)(k+3)}\right) c^{\{S\}} = \frac{1}{8}, \tag{21a}$$

$$e_{s^{\{S\}}}^T \left(\sum_{k=0}^{n_\Omega-1} \Omega^{\{k\}} \frac{1}{(k+1)(k+2)}\right) C^{\{S\}}c^{\{S\}} = \frac{1}{12}, \tag{21b}$$

$$e_{s^{\{S\}}}^T \Gamma C^{\{S\}} \left(\sum_{k=0}^{n_\Omega-1} \Omega^{\{k\}} \frac{1}{(k+1)(k+2)}\right) c^{\{S\}} = 0, \tag{21c}$$

$$e_{s^{\{S\}}}^T \overline{\Omega} C^{\{S\}} \left(\sum_{k=0}^{n_\Omega-1} \Omega^{\{k\}} \frac{1}{(k+1)(k+2)}\right) c^{\{S\}} = \frac{1}{24}, \tag{21d}$$

$$e_{s^{\{S\}}}^T \left(\sum_{k=0}^{n_\Omega-1} \Omega^{\{k\}} \frac{1}{(k+1)(k+2)}\right) \overline{\Omega} c^{\{S\}} = \frac{1}{24}, \tag{21e}$$

$$e_{s^{\{S\}}}^T \left(\sum_{k=0}^{n_\Omega-1} \Omega^{\{k\}} \frac{1}{(k+1)(k+2)}\right) \Gamma c^{\{S\}} = 0. \tag{21f}$$

Proof. From [16], there are 26 fourth-order coupling conditions for a third-order GARK method with this structure; this further reduces to 21 when $\mathbf{A}^{\{F,E\}} = \mathbf{A}^{\{F,I\}}$. These GARK coupling conditions are:

$$\left(\mathbf{b}^{\{\sigma\}}\right)^T \mathbf{C}^{\{S\}}\mathbf{A}^{\{S,F\}}\mathbf{c}^{\{F\}} = \frac{1}{8} \tag{22a}$$

$$\left(\mathbf{b}^{\{\sigma\}}\right)^T \mathbf{A}^{\{S,\nu\}}\mathbf{A}^{\{S,F\}}\mathbf{c}^{\{F\}} = \frac{1}{24} \tag{22b}$$

$$\left(\mathbf{b}^{\{\sigma\}}\right)^T \mathbf{A}^{\{S,F\}}\mathbf{C}^{\{F\}}\mathbf{c}^{\{F\}} = \frac{1}{12} \tag{22c}$$

$$\left(\mathbf{b}^{\{\sigma\}}\right)^T \mathbf{A}^{\{S,F\}}\mathbf{A}^{\{F,F\}}\mathbf{c}^{\{F\}} = \frac{1}{24} \tag{22d}$$

$$\left(\mathbf{b}^{\{F\}}\right)^T \mathbf{C}^{\{F\}}\mathbf{A}^{\{F,\sigma\}}\mathbf{c}^{\{S\}} = \frac{1}{8} \tag{22e}$$

$$\left(\mathbf{b}^{\{F\}}\right)^T \mathbf{A}^{\{F,\sigma\}}\mathbf{C}^{\{S\}}\mathbf{c}^{\{S\}} = \frac{1}{12} \tag{22f}$$

$$\left(\mathbf{b}^{\{\sigma\}}\right)^T \mathbf{A}^{\{S,F\}}\mathbf{A}^{\{F,\nu\}}\mathbf{c}^{\{S\}} = \frac{1}{24} \tag{22g}$$

$$\left(\mathbf{b}^{\{F\}}\right)^T \mathbf{A}^{\{F,F\}}\mathbf{A}^{\{F,\sigma\}}\mathbf{c}^{\{S\}} = \frac{1}{24} \tag{22h}$$

$$\left(\mathbf{b}^{\{F\}}\right)^T \mathbf{A}^{\{F,\sigma\}}\mathbf{A}^{\{S,\nu\}}\mathbf{c}^{\{S\}} = \frac{1}{24} \tag{22i}$$

$$\left(\mathbf{b}^{\{F\}}\right)^T \mathbf{A}^{\{F,\sigma\}}\mathbf{A}^{\{S,F\}}\mathbf{c}^{\{F\}} = \frac{1}{24} \tag{22j}$$

for $\sigma, \nu \in \{I, E\}$. $\mathbf{c}^{\{F\}}$ and $\mathbf{c}^{\{S\}}$ are defined as in (20a) and (20b), respectively. We arrive at the conditions (21) by checking each of the conditions (22) in turn.

The first four conditions (22a)–(22d) are automatically satisfied:

$$\begin{aligned}
\frac{1}{8} &= \left(\mathbf{b}^{\{\sigma\}}\right)^T \mathbf{C}^{\{S\}}\mathbf{A}^{\{S,F\}}\mathbf{c}^{\{F\}} \\
&= \left(b^{\{\sigma\}}\right)^T C^{\{S\}} \left(C^{\{S\}} \otimes \left(b^{\{F\}}\right)^T\right)\left(c^{\{S\}} \otimes c^{\{F\}}\right) \\
&= \left(b^{\{\sigma\}}\right)^T C^{\{S\}}C^{\{S\}}c^{\{S\}}\frac{1}{2} = \frac{1}{4}\cdot\frac{1}{2}, \\
\frac{1}{24} &= \left(\mathbf{b}^{\{\sigma\}}\right)^T \mathbf{A}^{\{S,\nu\}}\mathbf{A}^{\{S,F\}}\mathbf{c}^{\{F\}} \\
&= \left(b^{\{\sigma\}}\right)^T A^{\{\nu\}} \left(C^{\{S\}} \otimes \left(b^{\{F\}}\right)^T\right)\left(c^{\{S\}} \otimes c^{\{F\}}\right) \\
&= \left(b^{\{\sigma\}}\right)^T A^{\{\nu\}}C^{\{S\}}c^{\{S\}}\frac{1}{2} = \frac{1}{12}\cdot\frac{1}{2}, \\
\frac{1}{12} &= \left(\mathbf{b}^{\{\sigma\}}\right)^T \mathbf{A}^{\{S,F\}}\mathbf{C}^{\{F\}}\mathbf{c}^{\{F\}} \\
&= \left(b^{\{\sigma\}}\right)^T \left(C^{\{S\}} \otimes \left(b^{\{F\}}\right)^T\right)\operatorname{diag}\left(c^{\{S\}} \otimes c^{\{F\}}\right)\left(c^{\{S\}} \otimes c^{\{F\}}\right) \\
&= \left(b^{\{\sigma\}}\right)^T C^{\{S\}}C^{\{S\}}c^{\{S\}}\frac{1}{3} = \frac{1}{4}\cdot\frac{1}{3}, \\
\frac{1}{24} &= \left(\mathbf{b}^{\{\sigma\}}\right)^T \mathbf{A}^{\{S,F\}}\mathbf{A}^{\{F,F\}}\mathbf{c}^{\{F\}} \\
&= \left(b^{\{\sigma\}}\right)^T \left(C^{\{S\}} \otimes \left(b^{\{F\}}\right)^T\right)\left(C^{\{S\}} \otimes A^{\{F\}}\right)\left(c^{\{S\}} \otimes c^{\{F\}}\right) \\
&= \left(b^{\{\sigma\}}\right)^T C^{\{S\}}C^{\{S\}}c^{\{S\}}\frac{1}{6} = \frac{1}{4}\cdot\frac{1}{6}.
\end{aligned}$$

Condition (22e) is not automatically satisfied and simplifies to (21a):

$$\begin{aligned}
\frac{1}{8} &= \left(\mathbf{b}^{\{F\}}\right)^T \mathbf{C}^{\{F\}}\mathbf{A}^{\{F,\sigma\}}\mathbf{c}^{\{S\}} \\
&= \left(e_{s^{\{S\}}} \otimes b^{\{F\}}\right)^T \operatorname{diag}\left(c^{\{S\}} \otimes c^{\{F\}}\right)\left(\sum_{k=0}^{n_\Omega - 1} \Omega^{\{k\}} \otimes A^{\{F\}}\left(c^{\{F\}}\right)^k\right)c^{\{S\}} \\
&= e_{s^{\{S\}}}^T \left(\sum_{k=0}^{n_\Omega - 1} \Omega^{\{k\}}\frac{1}{(k+1)(k+3)}\right)c^{\{S\}}.
\end{aligned}$$

Condition (22f) is not automatically satisfied and simplifies to (21b).

$$\begin{aligned}
\frac{1}{12} &= \left(\mathbf{b}^{\{F\}}\right)^T \mathbf{A}^{\{F,\sigma\}}\mathbf{C}^{\{S\}}\mathbf{c}^{\{S\}} \\
&= \left(e_{s^{\{S\}}} \otimes b^{\{F\}}\right)^T \left(\sum_{k=0}^{n_\Omega - 1} \Omega^{\{k\}} \otimes A^{\{F\}}\left(c^{\{F\}}\right)^k\right)C^{\{S\}}c^{\{S\}} \\
&= e_{s^{\{S\}}}^T \left(\sum_{k=0}^{n_\Omega - 1} \Omega^{\{k\}}\frac{1}{(k+1)(k+2)}\right)C^{\{S\}}c^{\{S\}}.
\end{aligned}$$

Condition (22g) is not automatically satisfied and reduces to (21c) and (21d) when $\sigma = I, E$, respectively, and both conditions are enforced simultaneously,

$$\begin{aligned}\frac{1}{24} &= \left(\mathbf{b}^{\{\sigma\}}\right)^T \mathbf{A}^{\{S,F\}}\mathbf{A}^{\{F,\nu\}}\mathbf{c}^{\{S\}} \\ &= \left(b^{\{\sigma\}}\right)^T (C^{\{S\}} \otimes b^{\{F\}}) \left(\sum_{k=0}^{n_\Omega-1} \Omega^{\{k\}} \otimes A^{\{F\}} \left(c^{\{F\}}\right)^k\right) c^{\{S\}} \\ &= \left(b^{\{\sigma\}}\right)^T C^{\{S\}} \left(\sum_{k=0}^{n_\Omega-1} \Omega^{\{k\}} \frac{1}{(k+1)(k+2)}\right) c^{\{S\}}.\end{aligned}$$

Condition (22h) is not automatically satisfied but simplifies to (18) minus (21a),

$$\begin{aligned}\frac{1}{24} &= \left(\mathbf{b}^{\{F\}}\right)^T \mathbf{A}^{\{F,F\}}\mathbf{A}^{\{F,\sigma\}}\mathbf{c}^{\{S\}} \\ &= (e_{s\{S\}} \otimes b^{\{F\}})^T (C^{\{S\}} \otimes A^{\{F\}}) \left(\sum_{k=0}^{n_\Omega-1} \Omega^{\{k\}} \otimes A^{\{F\}} \left(c^{\{F\}}\right)^k\right) c^{\{S\}} \\ &= e_{s\{S\}}^T \left(\sum_{k=0}^{n_\Omega-1} \Omega^{\{k\}} \frac{1}{(k+1)(k+2)(k+3)}\right) c^{\{S\}}.\end{aligned}$$

Condition (22i) is not automatically satisfied and reduces to (21e) and (21f) when $\nu = I, E$, respectively, and both conditions are enforced simultaneously:

$$\begin{aligned}\frac{1}{24} &= \left(\mathbf{b}^{\{F\}}\right)^T \mathbf{A}^{\{F,\sigma\}}\mathbf{A}^{\{S,\nu\}}\mathbf{c}^{\{S\}} \\ &= (e_{s\{S\}} \otimes b^{\{F\}})^T \left(\sum_{k=0}^{n_\Omega-1} \Omega^{\{k\}} \otimes A^{\{F\}} \left(c^{\{F\}}\right)^k\right) \mathbf{A}^{\{S,\nu\}} c^{\{S\}} \\ &= e_{s\{S\}}^T \left(\sum_{k=0}^{n_\Omega-1} \Omega^{\{k\}} \frac{1}{(k+1)(k+2)}\right) \mathbf{A}^{\{S,\nu\}} c^{\{S\}}.\end{aligned}$$

Finally, condition (22j) simplifies to the same condition as (21b),

$$\begin{aligned}\frac{1}{24} &= \left(\mathbf{b}^{\{F\}}\right)^T \mathbf{A}^{\{F,\sigma\}}\mathbf{A}^{\{S,F\}}\mathbf{c}^{\{F\}} \\ &= (e_{s\{S\}} \otimes b^{\{F\}}) \left(\sum_{k=0}^{n_\Omega-1} \Omega^{\{k\}} \otimes A^{\{F\}} \left(c^{\{F\}}\right)^k\right) (C^{\{S\}} \otimes b^{\{F\}})(c^{\{S\}} \otimes c^{\{F\}}) \\ &= e_{s\{S\}}^T \left(\sum_{k=0}^{n_\Omega-1} \Omega^{\{k\}} \frac{1}{(k+1)(k+2)}\right) C^{\{S\}} c^{\{S\}} \frac{1}{2}.\end{aligned}$$

Theorem 4 (*Minimum n_Ω for Third-order Accuracy*)**.** *An IMEX-MRI-SR method requires at least $n_\Omega = 2$ for third-order accuracy.*

Proof. An IMEX-MRI-SR method with one Ω matrix, $\Omega^{\{0\}}$, has $\mathbf{A}^{\{S,E\}} = \overline{\Omega} = \Omega^0$ and, from the FSAL property, $\left(\mathbf{b}^{\{E\}}\right)^T = e_{s\{S\}}^T \overline{\Omega} = e_{s\{S\}}^T \Omega^{\{0\}}$. For an IMEX-MRI-SR method of order p, we assume the slow-explicit base method also satisfies all standard Runge–Kutta order conditions up to order p. Thus, a third-order IMEX-MRI-SR slow-explicit base method with one Ω satisfies the second order condition $\left(b^{\{E\}}\right)^T c^{\{S\}} = \frac{1}{2}$, which simplifies to

$$\frac{1}{2} = \sum_{j=1}^{s^{\{S\}}} \omega_{s\{S\},j}^{\{0\}} c_j^{\{S\}}.$$

However, the third-order IMEX-MRI-SR coupling condition (18) simplifies to

$$\frac{1}{3} = \sum_{j=1}^{s^{\{S\}}} \omega_{s\{S\},j}^{\{0\}} c_j^{\{S\}}.$$

Since these cannot hold simultaneously, a third-order IMEX-MRI-SR method with one Ω matrix is not possible. There are no such mutually exclusive conditions for $n_\Omega > 1$, and in Section 4 we introduce a third order method with $n_\Omega = 2$.

3. Linear stability

As in [13,16], we analyze the stability of IMEX-MRI-SR methods when applied to the linear, scalar test problem

$$y'(t) = \lambda^{\{F\}} y + \lambda^{\{E\}} y + \lambda^{\{I\}} y, \quad t \geq 0, \quad y(0) = 1, \tag{23}$$

with $\lambda^{\{F\}}, \lambda^{\{E\}}, \lambda^{\{I\}} \in \mathbb{C}^-$. For convenience, we additionally define $z^{\{F\}} = H\lambda^{\{F\}}$, $z^{\{E\}} = H\lambda^{\{E\}}$, and $z^{\{I\}} = H\lambda^{\{I\}}$. When applied to (23), the IVP (5b) becomes

$$\begin{aligned} v_i'(\theta) &= \lambda^{\{F\}} v_i(\theta) + \frac{1}{c_i^{\{S\}}} \sum_{j=1}^{i-1} \omega_{i,j} \left(\frac{\theta}{c_i^{\{S\}} H} \right) (\lambda^{\{E\}} Y_j^{\{S\}} + \lambda^{\{I\}} Y_j^{\{S\}}) \\ &= \lambda^{\{F\}} v_i(\theta) + \frac{1}{c_i^{\{S\}}} \sum_{j=1}^{i-1} \sum_{k=0}^{n_\Omega - 1} \omega_{i,j}^{\{k\}} \left(\frac{\theta}{c_i^{\{S\}} H} \right)^k (\lambda^{\{E\}} Y_j^{\{S\}} + \lambda^{\{I\}} Y_j^{\{S\}}) \end{aligned}$$

for $i = 2, \ldots, s^{\{S\}}$, with $\theta \in [0, c_i^{\{S\}} H]$ and $v_i(0) = y_n$. The solution to this at $\theta = c_i^{\{S\}} H$ is

$$\begin{aligned} v_i(c_i^{\{S\}} H) &= e^{c_i^{\{S\}} z^{\{F\}}} y_n + (z^{\{E\}} + z^{\{I\}}) \sum_{j=1}^{i-1} \sum_{k=0}^{n_\Omega - 1} \omega_{i,j}^{\{k\}} \left(\int_0^1 e^{c_i^{\{S\}} z^{\{F\}} (1-t)} t^k \mathrm{d}t \right) Y_j^{\{S\}} \\ &= \varphi_0(c_i^{\{S\}} z^{\{F\}}) y_n + (z^{\{E\}} + z^{\{I\}}) \sum_{j=1}^{i-1} \eta_{i,j}(z^{\{F\}}) Y_j^{\{S\}}. \end{aligned}$$

Here we define η as in [16] as a function of the fast eigenvalue $z^{\{F\}}$,

$$\eta_{i,j}(z^{\{F\}}) = \sum_{k=0}^{n_\Omega - 1} \omega_{i,j}^{\{k\}} \varphi_{k+1}(c_i^{\{S\}} z^{\{F\}}), \tag{24}$$

where the family of analytical functions $\{\varphi_k\}$ are given by [13],

$$\varphi_0(z) = e^z, \quad \varphi_k(z) = \int_0^1 e^{z(1-t)} t^{k-1} \mathrm{d}t, \quad k \geq 1.$$

The ith IMEX-MRI-SR stage for the stability problem (23) then becomes

$$Y_i^{\{S\}} = \varphi_0(c_i^{\{S\}} z^{\{F\}}) y_n + (z^{\{E\}} + z^{\{I\}}) \sum_{j=1}^{i-1} \eta_{i,j}(z^{\{F\}}) Y_j^{\{S\}} + z^{\{I\}} \sum_{j=1}^{i} \gamma_{i,j} Y_j^{\{S\}}. \tag{25}$$

Concatenating $Y = [Y_1^{\{S\}} \ \cdots \ Y_{s^{\{S\}}}^{\{S\}}]^T$ and writing (25) in matrix form,

$$\begin{aligned} Y &= \varphi_0(c^{\{S\}} z^{\{F\}}) y_n + (z^{\{E\}} + z^{\{I\}}) \eta(z^{\{F\}}) Y + z^{\{I\}} \Gamma Y \\ &= \left(I - (z^{\{E\}} + z^{\{I\}}) \eta(z^{\{F\}}) - z^{\{I\}} \Gamma \right)^{-1} \varphi_0(c^{\{S\}} z^{\{F\}}) y_n \end{aligned}$$

where

$$\eta(z^{\{F\}}) = \sum_{k=0}^{n_\Omega - 1} \mathrm{diag}(\varphi_{k+1}(c^{\{S\}} z^{\{F\}})) \Omega^{\{k\}}.$$

Thus the stability function for an IMEX-MRI-SR method applied to (23) is

$$R(z^{\{F\}}, z^{\{E\}}, z^{\{I\}}) = e_{s^{\{S\}}}^T \left(I - (z^{\{E\}} + z^{\{I\}}) \eta(z^{\{F\}}) - z^{\{I\}} \Gamma \right)^{-1} \varphi_0(c^{\{S\}} z^{\{F\}}). \tag{26}$$

We consider a few definitions of joint stability for IMEX-MRI-SR methods. As with IMEX-MRI-GARK methods, we consider a region that incorporates all three z,

$$\mathcal{J}_{\alpha,\rho,\beta,\xi} = \left\{ z^{\{E\}} \in \mathbb{C}^- : |R(z^{\{F\}}, z^{\{E\}}, z^{\{I\}})| \leq 1, \ \forall z^{\{F\}} \in \mathcal{S}_{\alpha,\rho}^{\{F\}}, \ \forall z^{\{I\}} \in \mathcal{S}_{\beta,\xi}^{\{I\}} \right\}, \tag{27}$$

where $\mathcal{S}_{\alpha,\rho}^{\{\sigma\}} = \left\{ z^{\{\sigma\}} \in \mathbb{C}^- : |\arg(z^{\{\sigma\}}) - \pi| \leq \alpha, \ |z^{\{\sigma\}}| \leq \rho \right\}$. We note that this definition of joint stability may be overly-restrictive, as it demands the implicit and fast parts of the method to be A(β)- and A(α)-stable, respectively, for any joint stability region to exist. Thus, we also analyze the implicit and explicit stability regions of IMEX-MRI-SR methods independently, with stability regions defined as:

$$\mathcal{J}_{\alpha,\rho}^{\{I\}} = \left\{ z^{\{I\}} \in \mathbb{C}^- : |R(z^{\{F\}}, 0, z^{\{I\}})| \leq 1, \ \forall z^{\{F\}} \in \mathcal{S}_{\alpha,\rho}^{\{F\}} \right\}, \tag{28}$$

$$\mathcal{J}^{\{E\}}_{\alpha,\rho} = \left\{ z^{\{E\}} \in \mathbb{C}^- : |R(z^{\{F\}}, z^{\{E\}}, 0)| \leq 1, \ \forall z^{\{F\}} \in \mathcal{S}^{\{F\}}_{\alpha,\rho} \right\}. \tag{29}$$

These are more consistent with standard stability analyses of ARK methods, wherein explicit and implicit stability are considered separately.

4. Example methods

We introduce IMEX-MRI-SR methods of orders 2 and 3, each of which includes an embedding with accuracy one order lower (1 and 2, resp.) for temporal error estimation. We also include discussion on fourth-order methods. We note that we designed the embedding coefficients with efficiency in mind, so that computation of the embedded solutions do not require an additional implicit solve at the slow time scale (i.e., $\hat{\gamma}_{s^{\{S\}}} = 0$).

When presenting the coefficients for each method we use the notation

$$\Omega^{\{k\}} = \left[\begin{array}{c} \boldsymbol{\Omega}^{\{\mathbf{k}\}} \\ \hline \hat{\omega}^{\{k\}} \end{array}\right], \quad \Gamma = \left[\begin{array}{c} \boldsymbol{\Gamma} \\ \hline \hat{\gamma} \end{array}\right],$$

where $\boldsymbol{\Omega}^{\{\mathbf{k}\}}$ and $\boldsymbol{\Gamma}$ are the matrices of coefficients defining the primary method, and $\hat{\omega}^{\{k\}}$ and $\hat{\gamma}$ are the embedding row of coefficients.

4.1. IMEX-MRI-SR2(1)

The first method is second-order with a first-order embedding. It has 4 stages, $n_\Omega = 1$, and requires 3 slow implicit solves per step. The coefficients can be found in Appendix A.

To create this method, we determined the free coefficients of the primary method by maximizing the extent along the negative real axis of the stability region defined by (27). We performed this maximization process using *Mathematica*'s [28] `NMaximize` function with the extent of the stability region for a given set of values for the free coefficients computed using a bisection method. We experimented with a variety of values of the parameters α, ρ, β, ξ in (27) to find a method with the largest, most robust stability regions.

We then determined the free coefficients of the embedded method by minimizing the value of the C-statistic from Prince and Dormand [29],

$$C^{(p+1)} = \frac{\|\hat{\tau}^{(p+1)} - \tau^{(p+1)}\|_2}{\|\hat{\tau}^{(p)}\|_2}, \tag{30}$$

where $\tau^{(p)}$ is the vector of order condition residuals at order p for the primary method, $\hat{\tau}^{(p)}$ is the vector of order condition residuals at order p for the embedded method, and p is the order of the primary method (in this case, $p = 2$). The C-statistic gives an estimate of how much the error stemming from unsatisfied $(p+1)$-order conditions of the primary method corrupts the error estimate provided by the embedded method.

This method has large, robust stability regions. Figs. 1(a) and 1(b) show $\mathcal{J}_{\alpha,10^2,\beta,10^4}$ for $\alpha \in \{10°, 45°\}$ and varying β, along with the explicit slow base method's stability region. We see that the multirate method has a stability region essentially identical to the explicit slow base method when $\alpha = 10°$ for any value of $z^{\{I\}}$. When α grows to 45° we can see a decay of the stability region associated with the $\beta = 85°$, while the regions associated with smaller β values experience negligible decay, if any.

Fig. 1(c) shows $\mathcal{J}^{\{E\}}_{\alpha,10^2}$ for varying α. We see that when $z^{\{I\}} = 0$, the stability region is again large, with only a slight decay in area when $\alpha = 85°$.

Fig. 1(c) shows $\mathcal{J}^{\{I\}}_{\alpha,10^2}$ for varying α. When $z^{\{E\}} = 0$, the multirate method is A-stable for $0° \leq \alpha \leq 45°$. When α grows further to 65°, the region decays slightly but is still approximately A(80°)-stable. When $\alpha = 85°$, the stability region decays to an enclosed bubble similar to the regions in Fig. 1(c).

4.2. IMEX-MRI-SR3(2)

Our second method is third-order with a second-order embedding. It has 5 stages, $n_\Omega = 2$, and requires 4 implicit solves per step. The coefficients can be found in Appendix B.

To create this method, we determined the free coefficients for both the method and embedding as described in Section 4.1, this time using the C-statistic (30) with $p = 3$.

Figs. 2(a) and 2(b) show the relatively large joint stability regions $\mathcal{J}_{\alpha,10^2,\beta,10^4}$ for $\alpha = \{10°, 45°\}$, respectively, along with the explicit slow base method's stability region. Again, at $\alpha = 10°$ and lower values of β, the method is essentially as stable as the explicit slow base method. The areas of these stability regions decrease for higher values of β. When α grows to 45° in Fig. 2(b), the stability regions shrink slightly in comparison with $\alpha = 10°$ from Fig. 2(a).

Figs. 2(c) and 2(d) show $\mathcal{J}^{\{E\}}_{\alpha,10^2}$ and $\mathcal{J}^{\{I\}}_{\alpha,10^2}$ for varying α, respectively. We see that when $z^{\{I\}} = 0$, the stability region is reasonably large for smaller value of α, but the region shrinks as α grows; however, even for $\alpha = 85°$, the region retains a good extent along the imaginary axis. Similar to the second-order method, when $z^{\{E\}} = 0$, the stability region is A-stable for most values of α, only losing A-stability for $\alpha = 85°$, where the region decays to a rather large, yet enclosed, bubble.

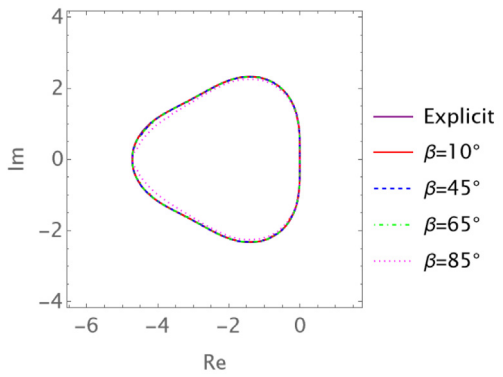

(a) $\mathcal{J}_{10°,10^2,\beta,10^4}$: When $z^{\{F\}}$ is allowed to vary within only 10° of the negative real axis, $\mathcal{J}$ largely retains its size as $z^{\{I\}}$ is allowed to vary closer to the imaginary axis.

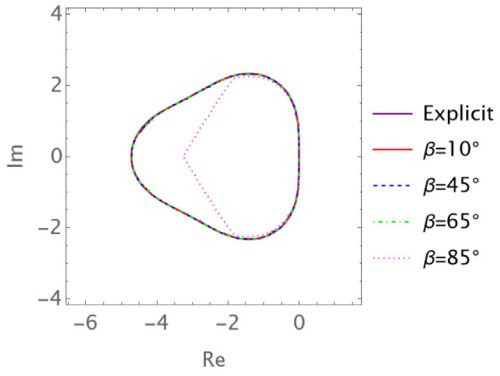

(b) $\mathcal{J}_{45°,10^2,\beta,10^4}$: When $z^{\{F\}}$ is allowed to vary within 45° of the negative real axis, $\mathcal{J}$ begins to decay when $z^{\{I\}}$ is allowed to vary closer to the imaginary axis.

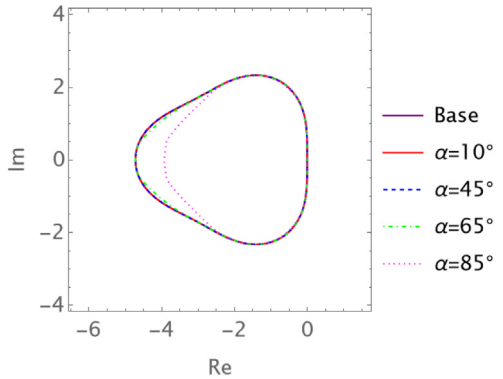

(c) $\mathcal{J}^{\{E\}}_{\alpha,10^2}$: $\mathcal{J}^{\{E\}}$ decays slightly as $z^{\{F\}}$ is allowed to vary closer to the imaginary axis.

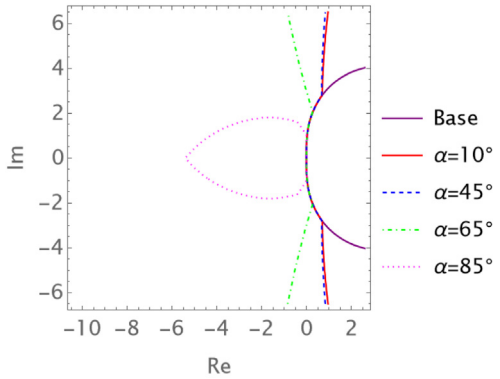

(d) $\mathcal{J}^{\{I\}}_{\alpha,10^2}$: $\mathcal{J}^{\{I\}}$ decays from A-stable to approximately A(80°)-stable to a finite region as $z^{\{F\}}$ is allowed to vary closer to the imaginary axis.

Fig. 1. Joint Stability Regions for IMEX-MRI-SR2(1).

4.3. Fourth-order Method

Deriving a fourth-order method by solving all order conditions simultaneously (as in Sections 4.1 and 4.2) proved to be a large computational challenge, due to the presence of many coupled high-degree polynomials, which caused the computer algebra system we used (*Mathematica*) to struggle.

We tried a variety of existing ARK methods as a base method to simplify the order conditions, as mentioned in Remark 2, which allowed us to derive a number of fourth-order methods. For these, we determined the free coefficients of the primary methods as in Section 4.1 but, because fifth-order conditions are not available, could not use the C-statistic for determining the embedding coefficients. The methods were derived with n_Ω as low as 2, demonstrating that fourth-order methods do not have a higher minimum value for n_Ω than third-order methods.

Our best method, derived using LIRK4 [23] as a base method, exhibited poor stability properties and poor numerical performance due to the aforementioned challenges. Consequently, we refrain from proposing any fourth order methods in this work. However, we provide the LIRK4-based method in the public numerical experiment repository provided in Section 6.

5. MERK methods as explicit IMEX-MRI-SR methods

In [8], Luan et al. define MERK methods with orders of accuracy spanning two through five by explicitly defining the abscissae $c_i^{\{S\}}$ and the forcing functions $g_i(\theta)$. Due to their similar structure to IMEX-MRI-SR methods, we may analyze

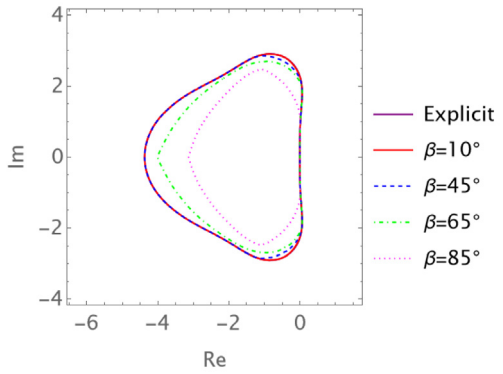

(a) $\mathcal{J}_{10^\circ,10^2,\beta,10^4}$: When $z^{\{F\}}$ is allowed to vary within only 10° of the negative real axis, $\mathcal{J}$ decays noticeably as $z^{\{I\}}$ is allowed to vary closer to the imaginary axis.

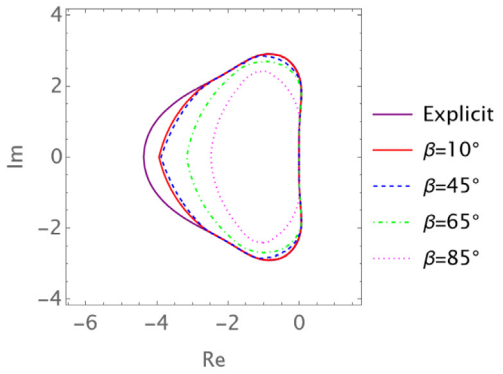

(b) $\mathcal{J}_{45^\circ,10^2,\beta,10^4}$: When $z^{\{F\}}$ is allowed to vary within 45° of the negative real axis, $\mathcal{J}$ decays significantly as $z^{\{I\}}$ is allowed to vary closer to the imaginary axis.

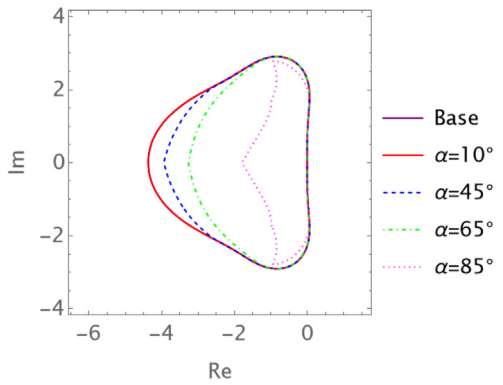

(c) $\mathcal{J}^{\{E\}}_{\alpha,10^2}$: $\mathcal{J}^{\{E\}}$ decays quickly as $z^{\{F\}}$ is allowed to vary closer to the imaginary axis.

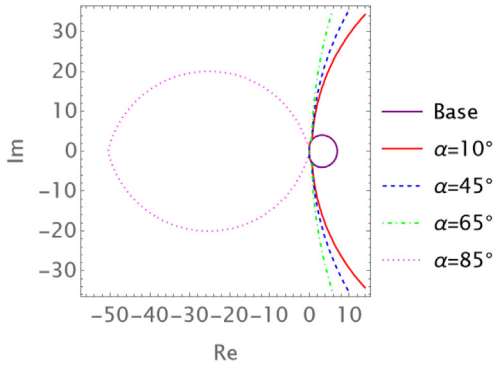

(d) $\mathcal{J}^{\{I\}}_{\alpha,10^2}$: $\mathcal{J}^{\{I\}}$ decays from A-stable to a rather large, yet finite region as $z^{\{F\}}$ is allowed to vary closer to the imaginary axis.

Fig. 2. Joint Stability Regions for IMEX-MRI-SR3(2)

MERK methods using our theory from Section 2. Because MERK methods are explicit, when writing them in IMEX-MRI-SR form they have zero-valued Γ matrices. We recall that MERK methods are defined under an assumption that the fast function is linear, $f^{\{F\}}(t,y) = \mathcal{L}y$. It is thus natural to assume that MERK methods might only satisfy a subset of the IMEX-MRI-SR order conditions, potentially failing those that handle nonlinearity in $f^{\{F\}}$.

5.1. MERK2

Converting the three-stage second-order accurate MERK2 method from [8] into IMEX-MRI-SR form, we have

$$\Omega^{\{0\}} = \begin{bmatrix} 0 & 0 & 0 \\ c_2^{\{S\}} & 0 & 0 \\ 1 & 0 & 0 \end{bmatrix}, \quad \Omega^{\{1\}} = \begin{bmatrix} 0 & 0 & 0 \\ 0 & 0 & 0 \\ -1/c_2^{\{S\}} & 1/c_2^{\{S\}} & 0 \end{bmatrix}. \tag{31}$$

Interestingly, these coefficients (along with $\Gamma = 0$) satisfy *all* coupling conditions up to third order, and the slow base method determined by $\overline{\Omega}$ satisfies all conditions up to order two. Thus, we expect MERK2 to have second-order accuracy, *even for nonlinear* $f^{\{F\}}$. We confirm this with numerical tests in Section 6, where we use $c_2^{\{S\}} = \frac{1}{2}$ since it was unspecified in [8].

Fig. 3(a) shows the stability regions for MERK2. Because this method is explicit, we only plot $\mathcal{J}^{\{E\}}_{\alpha,10^2}$. Notably, these regions nearly match that of the base explicit method for most values of α examined.

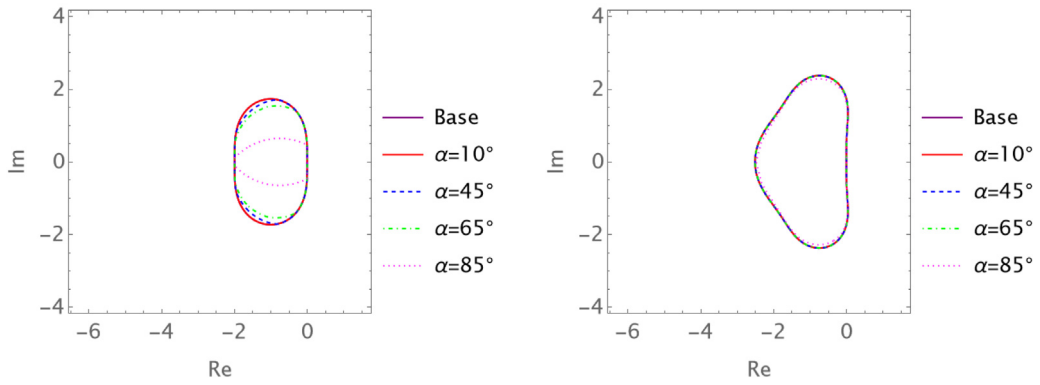

(a) MERK2: $\mathcal{J}^{\{E\}}$ decays as $z^{\{F\}}$ is allowed to vary closer to the imaginary axis.

(b) MERK3: $\mathcal{J}^{\{E\}}$ retains its size as $z^{\{F\}}$ is allowed to vary closer to the imaginary axis.

Fig. 3. $\mathcal{J}^{\{E\}}_{\alpha,10^2}$ Regions for MERK2 and MERK3.

5.2. MERK3

Converting the four-stage, third-order accurate, MERK3 from [8] to an IMEX-MRI-SR method, we have

$$\Omega^{\{0\}} = \begin{bmatrix} 0 & 0 & 0 & 0 \\ c_2^{\{S\}} & 0 & 0 & 0 \\ \frac{2}{3} & 0 & 0 & 0 \\ 1 & 0 & 0 & 0 \end{bmatrix}, \quad \Omega^{\{1\}} = \begin{bmatrix} 0 & 0 & 0 & 0 \\ 0 & 0 & 0 & 0 \\ -\frac{2}{3c_2^{\{S\}}} & \frac{2}{3c_2^{\{S\}}} & 0 & 0 \\ -\frac{3}{2} & 0 & \frac{3}{2} & 0 \end{bmatrix}. \tag{32}$$

These satisfy all coupling conditions up to third order, and the corresponding slow base method satisfies all conditions up to order three. Thus similarly to MERK2, we expect it to show third-order accuracy on problems with nonlinear $f^{\{F\}}$. We again confirm this result on numerical tests in Section 6 using $c_2^{\{S\}} = 1/2$.

Fig. 3(b) shows the stability regions for MERK3, $\mathcal{J}^{\{E\}}_{\alpha,10^2}$. Notably, these regions show no degradation of stability as α is increased.

5.3. MERK4

We may express MERK4 as an IMEX-MRI-SR method with 7 stages and $n_\Omega = 3$. The corresponding coefficients are provided in Appendix C.

We find that this method satisfies all IMEX-MRI-SR coupling conditions through order four, and its slow base method satisfies all order conditions up through fourth order, so long as $c_6^{\{S\}} = (3 - 4c_5^{\{S\}})/(4 - 6c_5^{\{S\}})$. This restriction on $c_6^{\{S\}}$ is satisfied by the choices in [8] of $c_2^{\{S\}} = 1/2$, $c_3^{\{S\}} = 1/2$, $c_4^{\{S\}} = 1/3$, $c_5^{\{S\}} = 5/6$, and $c_6^{\{S\}} = 1/3$. Thus like before, we expect this method to demonstrate fourth-order accuracy for nonlinear $f^{\{F\}}$, which we confirm numerically in Section 6. Interestingly, the joint stability regions $\mathcal{J}^{\{E\}}_{\alpha,10^2}$ for MERK4 are empty. However, given the reliability of this method in [8] and our own results from Section 6, we believe that these empty regions more strongly indicate a deficiency in these definitions of joint stability than any issues with MERK4 itself.

5.4. MERK5

The IMEX-MRI-SR method that corresponds with MERK5 has 11 stages and $n_\Omega = 4$. These coefficients are given in Appendix D. When analyzing this method, we find that when

$$c_9^{\{S\}} = \frac{12 - 15c_{10}^{\{S\}} - 15c_8^{\{S\}} + 20c_{10}^{\{S\}}c_8^{\{S\}}}{15 - 20c_{10}^{\{S\}} - 20c_8^{\{S\}} + 30c_{10}^{\{S\}}c_8^{\{S\}}}$$

the method satisfies all IMEX-MRI-SR coupling conditions up through fourth-order, and its slow base method satisfies all order conditions up through fifth-order. This condition is satisfied by the choice in [8] of $c_2^{\{S\}} = 1/2$, $c_3^{\{S\}} = 1/2$, $c_4^{\{S\}} = 1/3$, $c_5^{\{S\}} = 1/2$, $c_6^{\{S\}} = 1/3$, $c_7^{\{S\}} = 1/4$, $c_8^{\{S\}} = 7/10$, $c_9^{\{S\}} = 1/2$, and $c_{10}^{\{S\}} = 2/3$, therefore we expect it to have

at least fourth-order accuracy without restriction on the linearity of $f^{\{F\}}$. As we do not have fifth-order IMEX-MRI-SR order conditions, we cannot check these for MERK5; however, our numerical tests in Section 6 indeed show fifth-order convergence for nonlinear $f^{\{F\}}$. As with MERK4, the MERK5 joint stability regions $\mathcal{J}^{\{E\}}_{\alpha,10^2}$ are empty.

6. Numerical results

In this section we examine the convergence rates for our newly-proposed IMEX-MRI-SR methods from Section 4, as well as for MERK methods applied to problems with nonlinear $f^{\{F\}}$. We also compare the efficiency of our IMEX-MRI-SR methods against both IMEX-MRI-GARK and legacy Lie–Trotter and Strang–Marchuk methods from [16]. We omit the previously-published MERK methods from these performance comparisons because they do not support implicitness at the slow timescale. We provide a public GitHub repository for the code used in these numerical experiments: github.com/fishac/IMEXMRISRPaper.

All computations in this section were performed in serial utilizing nodes on Southern Methodist University's Maneframe2 supercomputer which each have a total of 36 cores over two Intel Xeon E5-2695 v4 CPUs. The computations were performed using C++ and the Armadillo [30,31] vector library.

6.1. Method configurations

In our numerical tests, we paired multirate methods with explicit fast Runge–Kutta methods of the same order, with the only exception of pairing a second-order fast solver with the first-order Lie–Trotter method. Each of Lie–Trotter, Strang–Marchuk, and IMEX-MRI-SR2(1) used the second-order Heun method. The IMEX-MRI-SR3(2) and IMEX-MRI-GARK3(a,b) methods used the third-order method by Bogacki and Shampine [32]. All implicit solves used a standard Newton–Raphson method with a banded linear solver.

We implemented the Lie–Trotter splitting method to take steps using function partitions in the order $f^{\{E\}}$, $f^{\{I\}}$, $f^{\{F\}}$ using Forward–Euler, Backward–Euler, and the second-order Heun method, respectively. The explicit and implicit steps used a step size of H and the fast step solved over an interval of size H.

Our Strang–Marchuk implementation used function partitions in the order $f^{\{E\}}, f^{\{I\}}, f^{\{F\}}, f^{\{I\}}, f^{\{E\}}$, using the second-order Heun method for the explicit steps, the implicit trapezoid rule for the implicit steps, and the second-order Heun method for the fast solve. The explicit and implicit steps used a step size of $H/2$ while the fast step solved over an interval of size H.

6.2. KPR

The Kværnø-Prothero–Robinson problem is a coupled system of IVPs which has been widely used for testing multirate algorithms, since it is nonlinear, non-autonomous, includes stiffness and multirate tuning parameters, and has an analytical solution. We use the same formulation and partitioning as in [16],

$$\begin{aligned} \begin{bmatrix} u' \\ v' \end{bmatrix} &= \Lambda \begin{bmatrix} \frac{-3+u^2-\cos(\beta t)}{2u} \\ \frac{-2+v^2-\cos(t)}{2v} \end{bmatrix} - \begin{bmatrix} \frac{\beta \sin(\beta t)}{2u} \\ \frac{\sin(t)}{2v} \end{bmatrix}, \quad \begin{bmatrix} u(0) \\ v(0) \end{bmatrix} = \begin{bmatrix} 2 \\ \sqrt{3} \end{bmatrix} \\ \Lambda &= \begin{bmatrix} \lambda^{\{F\}} & \frac{1-\varepsilon}{\alpha}(\lambda^{\{F\}} - \lambda^{\{S\}}) \\ -\alpha\varepsilon(\lambda^{\{F\}} - \lambda^{\{S\}}) & \lambda^{\{S\}} \end{bmatrix} \end{aligned} \tag{33}$$

for $t \in [0, 5\pi/2]$, with parameters $\lambda^{\{F\}} = -10$, $\lambda^{\{S\}} = -1$, $\varepsilon = 0.1$, $\alpha = 1$, and $\beta = 20$. This problem has solution

$$u(t) = \sqrt{3 + \cos(\beta t)}, \quad v(t) = \sqrt{2 + \cos(t)}. \tag{34}$$

We split the problem as

$$\begin{aligned} f^{\{E\}} &= \begin{bmatrix} 0 \\ \frac{\sin(t)}{2v} \end{bmatrix}, \quad f^{\{I\}} = \begin{bmatrix} 0 & 0 \\ 0 & 1 \end{bmatrix} \Lambda \begin{bmatrix} \frac{-3+u^2-\cos(\beta t)}{2u} \\ \frac{-2+v^2-\cos(t)}{2v} \end{bmatrix} \\ f^{\{F\}} &= \begin{bmatrix} 1 & 0 \\ 0 & 0 \end{bmatrix} \Lambda \begin{bmatrix} \frac{-3+u^2-\cos(\beta t)}{2u} \\ \frac{-2+v^2-\cos(t)}{2v} \end{bmatrix}. \end{aligned} \tag{35}$$

In Fig. 4, we plot the convergence as H is refined for MERK methods and implicit–explicit methods, including all provided IMEX-MRI-SR methods from Section 4, IMEX-MRI-GARK3(a,b), Lie–Trotter, and Strang–Marchuk. We see that all methods converge at their expected rates. Notably, as expected from Section 5, the MERK methods show no convergence issues even though $f^{\{F\}}$ in (35) is nonlinear.

We measured error at 10 equally-spaced points in the time interval. The estimated convergence rates for each method, using a least squares fit of log(Max Error) versus log(H), are in the legend parentheses. For the MERK convergence tests, we used $H = \pi/2^k$, $k = 2, \ldots, 9$ and for the implicit–explicit method convergence tests, we used $H = \pi/2^k$, $k = 4, \ldots, 11$. For all tests we used fast time step size $h = H/10$.

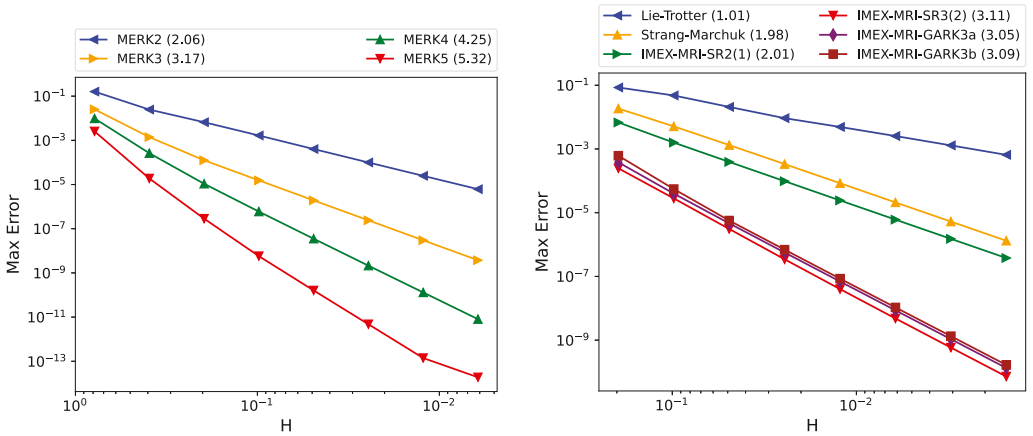

Fig. 4. Convergence for the KPR test problem (33) for MERK methods (left) and implicit–explicit methods (right) using the splitting (35). All methods converge at the expected theoretical rates (with measured convergence rates in parentheses), including MERK using nonlinear $f^{\{F\}}$.

6.3. Stiff brusselator

The stiff Brusselator problem is an advection-reaction–diffusion system of nonlinear partial differential equations. It is a modification to the standard Brusselator [33] used in [16], from which we use the same formulation and partitioning:

$$\begin{aligned} u_t &= \alpha_u u_{xx} + \rho_u u_x + r_u(a - (w-1)u + u^2 v), \\ v_t &= \alpha_v v_{xx} + \rho_v v_x + r_v(wu - u^2 v), \\ w_t &= \alpha_w w_{xx} + \rho_w w_x + r_w\left(\frac{b-w}{\varepsilon} - wu\right), \end{aligned}$$

for $t \in [0, 3]$ and $x \in [0, 1]$, with stationary boundary conditions

$$u_t(t,0) = u_t(t,1) = v_t(t,0) = v_t(t,1) = w_t(t,0) = w_t(t,1),$$

We partition the problem as

$$f^{\{I\}} = \begin{bmatrix} \alpha_u u_{xx} \\ \alpha_v v_{xx} \\ \alpha_w w_{xx} \end{bmatrix}, \quad f^{\{E\}} = \begin{bmatrix} \rho_u u_x \\ \rho_v v_x \\ \rho_w w_x \end{bmatrix}, \quad f^{\{F\}} = \begin{bmatrix} r_u(a - (w-1)u + u^2 v) \\ r_v(wu - u^2 v) \\ r_w(\frac{b-w}{\varepsilon} - wu) \end{bmatrix},$$

and use second order centered difference approximations for all spatial derivative operators. This problem has no analytical solution, so we used MATLAB's *ode15s* with tight tolerances *AbsTol* $= 10^{-14}$ and *RelTol* $= 2.5 \times 10^{-14}$ to generate reference solutions.

6.3.1. Fixed time step

In this section, we compare runtime efficiency of the splitting, IMEX-MRI-SR, and IMEX-MRI-GARK methods using fixed time step sizes. We use the same fixed parameters $\alpha_u = \alpha_v = \alpha_w = 10^{-2}$, $\rho_u = \rho_v = \rho_w = 10^{-3}$, $r_u = r_v = r_w = 1$, $a = 0.6$, $b = 2$, and $\varepsilon = 10^{-2}$ with initial conditions

$$u(0) = a + 0.1\sin(\pi x), \quad v(0) = b/a + 0.1\sin(\pi x), \quad w(0) = b + 0.1\sin(\pi x),$$

for 201 and 801 grid points as in [16]. All methods used fast time steps of $h = H/10$.

In Fig. 5 we plot the observed maximum solution error over ten equally spaced points in the time interval using step sizes of $H = 0.1 \cdot 2^{-k}$, $k = 0, \ldots, 10$. The second- and third-order IMEX-MRI-SR and IMEX-MRI-GARK methods all achieve their expected order for the 201 grid. The third-order accurate methods experience only slight order reduction for the 801 grid while IMEX-MRI-SR2(1) remains steady at its expected order. All third-order methods exhibit an error floor of approximately 10^{-11}, that is likely caused by the accuracy of the reference solution.

We can see that IMEX-MRI-SR2(1) is far more efficient than the first- and second-order operator splitting methods for this problem, providing errors two to three orders of magnitude smaller for the same runtimes. It also enters its asymptotic convergence regime at significantly larger step sizes than the operator splitting methods.

The third-order methods demonstrate the best efficiency for both grids, with IMEX-MRI-SR3(2) becoming the most efficient method for the 801 grid for errors between approximately 10^{-7} and 10^{-11}.

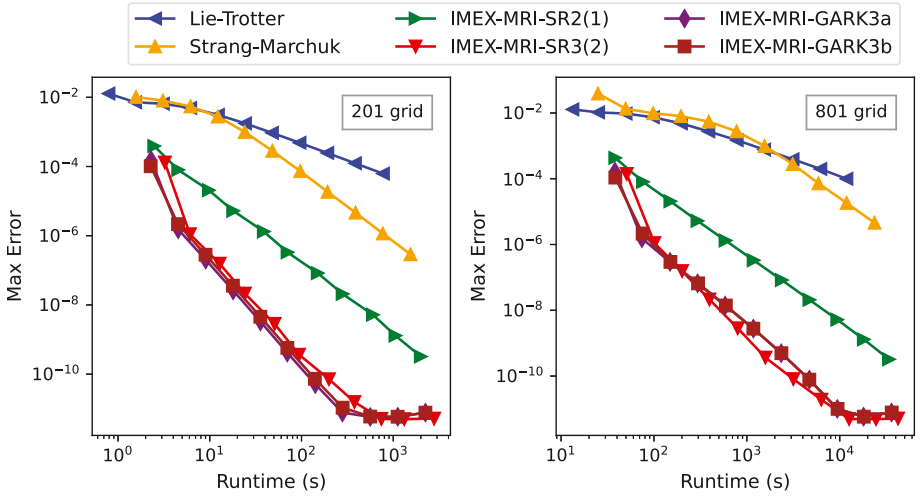

Fig. 5. Efficiency for stiff Brusselator problem using 201 grid points (left) and 801 grid points (right). Estimated least-squares convergence rates in the asymptotic convergence regime are (0.98,2.00,2.00,3.09,3.36,3.25) and (0.98,1.94,2.01,2.90,2.71,2.69) for the 201 and 801 grids, respectively, for Lie–Trotter, Strang–Marchuk, IMEX-MRI-SR2(1), IMEX-MRI-SR3(2), IMEX-MRI-GARK3a, IMEX-MRI-GARK3b.

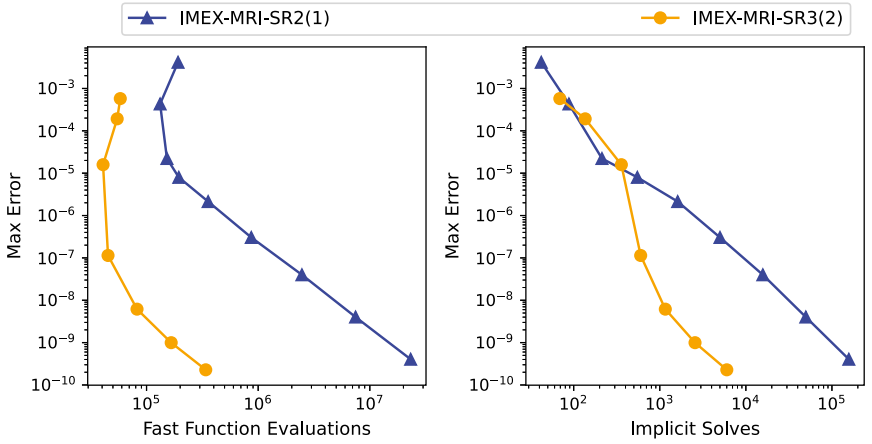

Fig. 6. Fast function evaluations (left) and total implicit solves (right) versus the observed maximum error for the stiff Brusselator problem.

6.3.2. Adaptive time step

In this section, we compare work-precision efficiency for the IMEX-MRI-SR methods in the adaptive time step context. Because the operator splitting and IMEX-MRI-GARK methods do not have embeddings, we omit them from these tests. We use the Constant-Constant controller from [34] with its recommended parameters $k_1 = 0.42$, $k_2 = 0.44$, and its recommended fast error measurement strategy, LASA-mean. This controller simultaneously adapts H and M (where the fast time step size is $h = H/M$) in a similar manner to standard single-rate I-controllers.

We use time-varying parameters $\alpha_u = \alpha_v = \alpha_w = \rho_u = \rho_v = \rho_w = 6 \times 10^{-5} + 5 \times 10^{-5} \cos(\pi t)$, $r_u = r_v = r_w = 0.6 + 0.5 \cos(4\pi t)$ adapted from [34] with the same fixed parameters $a = 1$, $b = 3.5$, $\varepsilon = 10^{-3}$ and initial conditions

$$u(0) = 1.2 + 0.1 \sin(\pi x), \quad v(0) = 3.1 + 0.1 \sin(\pi x), \quad w(0) = 3 + 0.1 \sin(\pi x),$$

with 101 grid points. All IMEX-MRI-SR methods used the same fast methods and implicit algebraic solvers as in Section 6.2.

In Fig. 6 we plot the number of fast function evaluations and the number of implicit solves, good indicators of overall cost at the fast and slow timescales, versus the observed maximum solution error over ten equally spaced points in the time interval when running with controller tolerance values of $\text{TOL} = 10^{-k}$, $k = 1, \ldots, 9$. We use $\text{TOL}^{\{S\}} = \text{TOL}^{\{F\}} = \frac{1}{2}\text{TOL}$ in our tests for simplicity. We note that IMEX-MRI-SR3(2) failed the tests with $\text{TOL} = 10^{-3}, 10^{-5}$ due to getting stuck in oscillations between successful and failed steps.

We can see that IMEX-MRI-SR2(1) is much less efficient than IMEX-MRI-SR3(2) in terms of fast function evaluations (farthest from the bottom-left corner). The total number of implicit solves is comparable across both methods for errors larger than approximately 10^{-5}. Below that, IMEX-MRI-SR2(1) falls behind.

7. Conclusions

We introduce a new class of multirate time integration methods which builds off of previous work in IMEX-MRI-GARK and MERK methods, serving to improve various aspects of each. The proposed class of IMEX-MRI-SR methods are flexible, allowing IMEX treatment of the slow time scale while allowing the use of any viable IVP solver for the fast time scale. These methods remove the sorted abscissae requirement of IMEX-MRI-GARK methods since they start each internal stage at the beginning of the time step, thereby dramatically simplifying their order conditions and allowing introduction of embeddings. IMEX-MRI-SR methods can also be viewed as an extension to MERK methods, in that these allow implicitness at the slow time scale and nonlinearity at the fast time scale.

The convergence theory of IMEX-MRI-SR methods leverages GARK theory [6], through which we established order conditions for methods of orders one through four. Due to their structural similarity to IMEX-MRI-SR methods, we leveraged these new order conditions to analyze the previously-proposed MERK methods without their restriction to linear fast partitions. Using this analytical framework, we provided the first theoretical justification that these MERK methods (at least up through fourth order) should retain their high orders of accuracy even on problems with nonlinear fast partitions.

Using this theoretical framework, we provided two new IMEX-MRI-SR methods. These included a second-order method with a first-order embedding, and a third-order method with a second-order embedding, both derived from scratch by solving all order conditions simultaneously.

We experimentally examined convergence for the two new methods and the existing MERK methods on the KPR test problem, finding that they all converge at their expected orders of accuracy. We also provided experimental efficiency results on the stiff Brusselator problem, a nonlinear advection-reaction–diffusion system of PDEs, where we found that our methods are competitive with IMEX-MRI-GARK methods and even surpass them in some cases. We also found that IMEX-MRI-SR2(1) is vastly more efficient than the similarly second-order Strang–Marchuk operator splitting method in our test problems. We found that in the context of adaptive time stepping for our test problem, IMEX-MRI-SR3(2) proved superior than IMEX-MRI-SR2(1).

More work remains to be done on IMEX-MRI-SR methods. Higher order conditions can be derived which, while tedious due to the number of conditions at higher orders, is tractable due to the use of Kronecker product identities. Further analysis should be done on the factors that most strongly affect joint stability and what conditions, if any, can be enforced to ensure a non-empty joint stability region. Additionally, more methods should be derived, in particular a high quality embedded fourth-order method.

Data availability

No data was used for the research described in the article.

Acknowledgments

The authors would like to thank Vu Thai Luan for his help in gaining deeper understanding of MERK methods. We would also like to thank the SMU Center for Research Computing for use of the Maneframe2 computing cluster, where we performed all simulations reported in this work

Appendix A. IMEX-MRI-SR2(1) coefficients

$$c^{\{S\}} = \begin{bmatrix} 0 \\ \frac{3}{5} \\ \frac{4}{15} \\ 1 \end{bmatrix}, \quad \Omega^{\{0\}} = \left[\begin{array}{cccc} 0 & 0 & 0 & 0 \\ \frac{3}{5} & 0 & 0 & 0 \\ \frac{14}{165} & \frac{2}{11} & 0 & 0 \\ -\frac{13}{54} & \frac{137}{270} & \frac{11}{15} & 0 \\ \hline -\frac{1}{4} & \frac{1}{2} & \frac{3}{4} & 0 \end{array}\right], \quad \Gamma = \left[\begin{array}{cccc} 0 & 0 & 0 & 0 \\ -\frac{11}{23} & \frac{11}{23} & 0 & 0 \\ -\frac{6692}{52371} & -\frac{18355}{52371} & \frac{11}{23} & 0 \\ \frac{11621}{90666} & -\frac{215249}{226665} & \frac{17287}{50370} & \frac{11}{23} \\ \hline -\frac{31}{12} & -\frac{1}{6} & \frac{11}{4} & 0 \end{array}\right]. \tag{A.1}$$

Appendix B. IMEX-MRI-SR3(2) coefficients

$$c^{\{S\}} = \begin{bmatrix} 0 \\ \frac{23}{34} \\ \frac{4}{5} \\ \frac{17}{15} \\ 1 \end{bmatrix}, \quad \Omega^{\{0\}} = \left[\begin{array}{ccccc} 0 & 0 & 0 & 0 & 0 \\ \frac{23}{34} & 0 & 0 & 0 & 0 \\ \frac{71}{70} & -\frac{3}{14} & 0 & 0 & 0 \\ \frac{124}{1155} & \frac{4}{7} & \frac{5}{11} & 0 & 0 \\ \frac{162181}{187680} & \frac{119}{1380} & \frac{11}{32} & -\frac{5}{17} & 0 \\ \hline \frac{76355}{74834} & -\frac{46}{31} & \frac{67}{34} & -\frac{36}{71} & 0 \end{array}\right],$$

$$\Omega^{\{1\}} = \left[\begin{array}{ccccc} 0 & 0 & 0 & 0 & 0 \\ 0 & 0 & 0 & 0 & 0 \\ -\frac{14453}{63825} & \frac{14453}{63825} & 0 & 0 & 0 \\ -\frac{2101267877}{1206582300} & -\frac{2476735438}{301645575} & -\frac{13575085}{2098404} & 0 & 0 \\ -\frac{762580446799}{588660102960} & \frac{11083240219}{4328383110} & -\frac{211274129}{100368304} & \frac{89562055}{106641323} & 0 \\ \hline -\frac{3732974}{2278035} & \frac{13857574}{2278035} & -\frac{52}{9} & \frac{4}{3} & 0 \end{array}\right], \tag{B.1}$$

$$\Gamma = \left[\begin{array}{ccccc} 0 & 0 & 0 & 0 & 0 \\ -\frac{4}{7} & \frac{4}{7} & 0 & 0 & 0 \\ -\frac{2707004}{3127425} & \frac{919904}{3127425} & \frac{4}{7} & 0 & 0 \\ \frac{852879271}{703839675} & -\frac{1575000496}{703839675} & \frac{5}{11} & \frac{4}{7} & 0 \\ \frac{43136869}{2019912118} & -\frac{73810600}{1009956059} & -\frac{17653551}{87822266} & -\frac{13993902}{43911133} & \frac{4}{7} \\ \hline -\frac{179}{4140} & \frac{799}{14490} & \frac{1}{14} & -\frac{1}{12} & 0 \end{array}\right]$$

Appendix C. MERK4 IMEX-MRI-SR coefficients

We list the non-zero coefficients of the MERK5 method's IMEX-MRI-SR formulation below.

$$\omega_{i,1}^{\{0\}} = c_i^{\{S\}}, \ i = 1, \ldots, s^{\{S\}} \tag{C.1}$$

$$\begin{aligned}
&\omega_{3,1}^{\{1\}} = -\omega_{3,2}^{\{1\}}, \ \omega_{3,2}^{\{1\}} = \frac{c_3^{\{S\}\times 2}}{c_2^{\{S\}}}, \ \omega_{4,1}^{\{1\}} = -\omega_{4,2}^{\{1\}}, \ \omega_{4,2}^{\{1\}} = \frac{c_4^{\{S\}\times 2}}{c_2^{\{S\}}}, \\
&\omega_{5,1}^{\{1\}} = -(\omega_{5,3}^{\{1\}} + \omega_{5,4}^{\{1\}}), \ \omega_{5,3}^{\{1\}} = -\frac{c_4^{\{S\}} c_5^{\{S\}\times 2}}{c_3^{\{S\}}(c_3^{\{S\}} - c_4^{\{S\}})}, \ \omega_{5,4}^{\{1\}} = \frac{c_3^{\{S\}} c_5^{\{S\}\times 2}}{c_4^{\{S\}}(c_3^{\{S\}} - c_4^{\{S\}})} \\
&\omega_{6,1}^{\{1\}} = -(\omega_{6,3}^{\{1\}} + \omega_{6,4}^{\{1\}}), \ \omega_{6,3}^{\{1\}} = -\frac{c_4^{\{S\}} c_6^{\{S\}\times 2}}{c_3^{\{S\}}(c_3^{\{S\}} - c_4^{\{S\}})}, \ \omega_{6,4}^{\{1\}} = \frac{c_3^{\{S\}} c_6^{\{S\}\times 2}}{c_4^{\{S\}}(c_3^{\{S\}} - c_4^{\{S\}})} \\
&\omega_{7,1}^{\{1\}} = -(\omega_{7,5}^{\{1\}} + \omega_{7,6}^{\{1\}}), \ \omega_{7,5}^{\{1\}} = -\frac{c_6^{\{S\}}}{c_5^{\{S\}}(c_5^{\{S\}} - c_6^{\{S\}})}, \ \omega_{7,6}^{\{1\}} = \frac{c_5^{\{S\}}}{c_6^{\{S\}}(c_5^{\{S\}} - c_6^{\{S\}})}
\end{aligned} \tag{C.2}$$

$$\begin{aligned}
&\omega_{5,1}^{\{1\}} = -(\omega_{5,3}^{\{1\}} + \omega_{5,4}^{\{1\}}), \ \omega_{5,3}^{\{1\}} = \frac{1}{c_3^{\{S\}}(c_3^{\{S\}} - c_4^{\{S\}})}, \ \omega_{5,4}^{\{1\}} = -\frac{1}{c_4^{\{S\}}(c_3^{\{S\}} - c_4^{\{S\}})} \\
&\omega_{6,1}^{\{1\}} = -(\omega_{6,3}^{\{1\}} + \omega_{6,4}^{\{1\}}), \ \omega_{6,3}^{\{1\}} = \frac{1}{c_3^{\{S\}}(c_3^{\{S\}} - c_4^{\{S\}})}, \ \omega_{6,4}^{\{1\}} = -\frac{1}{c_4^{\{S\}}(c_3^{\{S\}} - c_4^{\{S\}})} \\
&\omega_{7,1}^{\{1\}} = -(\omega_{7,5}^{\{1\}} + \omega_{7,6}^{\{1\}}), \ \omega_{7,5}^{\{1\}} = \frac{1}{c_5^{\{S\}}(c_5^{\{S\}} - c_6^{\{S\}})}, \ \omega_{7,6}^{\{1\}} = -\frac{1}{c_6^{\{S\}}(c_5^{\{S\}} - c_6^{\{S\}})}
\end{aligned} \tag{C.3}$$

This method attains general fourth-order accuracy when

$$c_6^{\{S\}} = \frac{3 - 4c_5^{\{S\}}}{4 - 6c_5^{\{S\}}}. \tag{C.4}$$

Appendix D. MERK5 IMEX-MRI-SR coefficients

We list the non-zero coefficients of the MERK5 method's IMEX-MRI-SR formulation below.

$$\omega^{\{0\}}_{i,1} = c^{\{S\}}_i,\ i = 1, \ldots, s^{\{S\}} \tag{D.1}$$

$$\begin{aligned}
&\omega^{\{1\}}_{3,1} = -\omega^{\{1\}}_{3,2},\ \omega^{\{1\}}_{3,2} = c_3^{\{S\}\times 2}\alpha_2,\\
&\omega^{\{1\}}_{4,1} = -\omega^{\{1\}}_{4,2},\ \omega^{\{1\}}_{4,2} = c_4^{\{S\}\times 2}\alpha_2,\\
&\omega^{\{1\}}_{5,1} = -\left(\omega^{\{1\}}_{5,3} + \omega^{\{1\}}_{5,4}\right),\ \omega^{\{1\}}_{5,3} = c_5^{\{S\}\times 2}\alpha_3,\ \omega^{\{1\}}_{5,4} = c_5^{\{S\}\times 2}\alpha_4\\
&\omega^{\{1\}}_{6,1} = -\left(\omega^{\{1\}}_{6,3} + \omega^{\{1\}}_{6,4}\right),\ \omega^{\{1\}}_{6,3} = c_6^{\{S\}\times 2}\alpha_3,\ \omega^{\{1\}}_{6,4} = c_6^{\{S\}\times 2}\alpha_4\\
&\omega^{\{1\}}_{7,1} = -\left(\omega^{\{1\}}_{7,3} + \omega^{\{1\}}_{7,4}\right),\ \omega^{\{1\}}_{7,3} = c_7^{\{S\}\times 2}\alpha_3,\ \omega^{\{1\}}_{7,4} = c_7^{\{S\}\times 2}\alpha_4\\
&\omega^{\{1\}}_{8,1} = -\left(\omega^{\{1\}}_{8,5} + \omega^{\{1\}}_{8,6} + \omega^{\{1\}}_{8,7}\right),\ \omega^{\{1\}}_{8,5} = c_8^{\{S\}\times 2}\alpha_5,\ \omega^{\{1\}}_{8,6} = c_8^{\{S\}\times 2}\alpha_6,\ \omega^{\{1\}}_{8,7} = c_8^{\{S\}\times 2}\alpha_7\\
&\omega^{\{1\}}_{9,1} = -\left(\omega^{\{1\}}_{9,5} + \omega^{\{1\}}_{9,6} + \omega^{\{1\}}_{9,7}\right),\ \omega^{\{1\}}_{9,5} = c_9^{\{S\}\times 2}\alpha_5,\ \omega^{\{1\}}_{9,6} = c_9^{\{S\}\times 2}\alpha_6,\ \omega^{\{1\}}_{9,7} = c_9^{\{S\}\times 2}\alpha_7\\
&\omega^{\{1\}}_{10,1} = -\left(\omega^{\{1\}}_{10,5} + \omega^{\{1\}}_{10,6} + \omega^{\{1\}}_{10,7}\right),\ \omega^{\{1\}}_{10,5} = c_{10}^{\{S\}\times 2}\alpha_5,\ \omega^{\{1\}}_{10,6} = c_{10}^{\{S\}\times 2}\alpha_6,\ \omega^{\{1\}}_{10,7} = c_{10}^{\{S\}\times 2}\alpha_7\\
&\omega^{\{1\}}_{11,1} = -\left(\omega^{\{1\}}_{11,8} + \omega^{\{1\}}_{11,9} + \omega^{\{1\}}_{11,10}\right),\ \omega^{\{1\}}_{11,8} = \alpha_8,\ \omega^{\{1\}}_{11,9} = \alpha_9,\ \omega^{\{1\}}_{11,10} = \alpha_{10}
\end{aligned} \tag{D.2}$$

where

$$\begin{aligned}
&\alpha_2 = \frac{1}{c_2^{\{S\}}},\ \alpha_3 = \frac{c_3^{\{S\}}}{c_3^{\{S\}}(c_4^{\{S\}} - c_3^{\{S\}})},\ \alpha_4 = \frac{c_4^{\{S\}}}{c_4^{\{S\}}(c_3^{\{S\}} - c_4^{\{S\}})}\\
&\alpha_5 = \frac{c_6^{\{S\}}c_7^{\{S\}}}{c_5^{\{S\}}(c_5^{\{S\}} - c_6^{\{S\}})(c_5^{\{S\}} - c_7^{\{S\}})},\ \alpha_6 = \frac{c_5^{\{S\}}c_7^{\{S\}}}{c_6^{\{S\}}(c_6^{\{S\}} - c_5^{\{S\}})(c_6^{\{S\}} - c_7^{\{S\}})},\\
&\alpha_7 = \frac{c_5^{\{S\}}c_6^{\{S\}}}{c_7^{\{S\}}(c_7^{\{S\}} - c_5^{\{S\}})(c_7^{\{S\}} - c_6^{\{S\}})},\ \alpha_8 = \frac{c_9^{\{S\}}c_{10}^{\{S\}}}{c_8^{\{S\}}(c_8^{\{S\}} - c_9^{\{S\}})(c_8^{\{S\}} - c_{10}^{\{S\}})}\\
&\alpha_9 = \frac{c_8^{\{S\}}c_{10}^{\{S\}}}{c_9^{\{S\}}(c_9^{\{S\}} - c_8^{\{S\}})(c_9^{\{S\}} - c_{10}^{\{S\}})},\ \alpha_{10} = \frac{c_8^{\{S\}}c_9^{\{S\}}}{c_{10}^{\{S\}}(c_{10}^{\{S\}} - c_8^{\{S\}})(c_{10}^{\{S\}} - c_9^{\{S\}})}
\end{aligned} \tag{D.3}$$

$$\begin{aligned}
&\omega^{\{2\}}_{5,1} = -\left(\omega^{\{2\}}_{5,3} + \omega^{\{2\}}_{5,4}\right),\ \omega^{\{2\}}_{5,3} = c_5^{\{S\}\times 2}\beta_3,\ \omega^{\{2\}}_{5,4} = -c_5^{\{S\}\times 2}\beta_4\\
&\omega^{\{2\}}_{6,1} = -\left(\omega^{\{2\}}_{6,3} + \omega^{\{2\}}_{6,4}\right),\ \omega^{\{2\}}_{6,3} = c_6^{\{S\}\times 2}\beta_3,\ \omega^{\{2\}}_{6,4} = -c_6^{\{S\}\times 2}\beta_4\\
&\omega^{\{2\}}_{7,1} = -\left(\omega^{\{2\}}_{7,3} + \omega^{\{2\}}_{7,4}\right),\ \omega^{\{2\}}_{7,3} = c_7^{\{S\}\times 2}\beta_3,\ \omega^{\{2\}}_{7,4} = -c_7^{\{S\}\times 2}\beta_4\\
&\omega^{\{2\}}_{8,1} = -\left(\omega^{\{2\}}_{8,5} + \omega^{\{2\}}_{8,6} + \omega^{\{2\}}_{8,7}\right),\ \omega^{\{2\}}_{8,5} = -c_8^{\{S\}\times 2}\beta_5,\ \omega^{\{2\}}_{8,6} = -c_8^{\{S\}\times 2}\beta_6,\ \omega^{\{2\}}_{8,7} = -c_8^{\{S\}\times 2}\beta_7\\
&\omega^{\{2\}}_{9,1} = -\left(\omega^{\{2\}}_{9,5} + \omega^{\{2\}}_{9,6} + \omega^{\{2\}}_{9,7}\right),\ \omega^{\{2\}}_{9,5} = -c_9^{\{S\}\times 2}\beta_5,\ \omega^{\{2\}}_{9,6} = -c_9^{\{S\}\times 2}\beta_6,\ \omega^{\{2\}}_{9,7} = -c_9^{\{S\}\times 2}\beta_7\\
&\omega^{\{2\}}_{10,1} = -\left(\omega^{\{2\}}_{10,5} + \omega^{\{2\}}_{10,6} + \omega^{\{2\}}_{10,7}\right),\ \omega^{\{2\}}_{10,5} = -c_{10}^{\{S\}\times 2}\beta_5,\ \omega^{\{2\}}_{10,6} = -c_{10}^{\{S\}\times 2}\beta_6,\ \omega^{\{2\}}_{10,7} = -c_{10}^{\{S\}\times 2}\beta_7\\
&\omega^{\{2\}}_{11,1} = -\left(\omega^{\{2\}}_{11,8} + \omega^{\{2\}}_{11,9} + \omega^{\{2\}}_{11,10}\right),\ \omega^{\{2\}}_{11,8} = \beta_8,\ \omega^{\{2\}}_{11,9} = \beta_9,\ \omega^{\{2\}}_{11,10} = \beta_{10}
\end{aligned} \tag{D.4}$$

where

$$\begin{aligned}
&\beta_3 = \frac{1}{c_3^{\{S\}}(c_4^{\{S\}} - c_3^{\{S\}})},\ \beta_4 = \frac{1}{c_4^{\{S\}}(c_3^{\{S\}} - c_4^{\{S\}})}\\
&\beta_5 = \frac{c_6^{\{S\}} + c_7^{\{S\}}}{c_5^{\{S\}}(c_5^{\{S\}} - c_6^{\{S\}})(c_5^{\{S\}} - c_7^{\{S\}})},\ \beta_6 = \frac{c_5^{\{S\}} + c_7^{\{S\}}}{c_6^{\{S\}}(c_6^{\{S\}} - c_5^{\{S\}})(c_6^{\{S\}} - c_7^{\{S\}})},\\
&\beta_7 = \frac{c_5^{\{S\}} + c_6^{\{S\}}}{c_7^{\{S\}}(c_7^{\{S\}} - c_5^{\{S\}})(c_7^{\{S\}} - c_6^{\{S\}})},\ \beta_8 = \frac{c_9^{\{S\}} + c_{10}^{\{S\}}}{c_8^{\{S\}}(c_8^{\{S\}} - c_9^{\{S\}})(c_8^{\{S\}} - c_{10}^{\{S\}})}\\
&\beta_9 = \frac{c_8^{\{S\}} + c_{10}^{\{S\}}}{c_9^{\{S\}}(c_9^{\{S\}} - c_8^{\{S\}})(c_9^{\{S\}} - c_{10}^{\{S\}})},\ \beta_{10} = \frac{c_8^{\{S\}} + c_9^{\{S\}}}{c_{10}^{\{S\}}(c_{10}^{\{S\}} - c_8^{\{S\}})(c_{10}^{\{S\}} - c_9^{\{S\}})}
\end{aligned} \tag{D.5}$$

$$\begin{aligned}
\omega^{\{3\}}_{8,1} &= -\left(\omega^{\{3\}}_{8,5}+\omega^{\{3\}}_{8,6}+\omega^{\{3\}}_{8,7}\right),\ \omega^{\{3\}}_{8,5}=c^{\{S\}\times 2}_{8}\gamma_5,\ \omega^{\{3\}}_{8,6}=c^{\{S\}\times 2}_{8}\gamma_6,\ \omega^{\{3\}}_{8,7}=c^{\{S\}\times 2}_{8}\gamma_7\\
\omega^{\{3\}}_{9,1} &= -\left(\omega^{\{3\}}_{9,5}+\omega^{\{3\}}_{9,6}+\omega^{\{3\}}_{9,7}\right),\ \omega^{\{3\}}_{9,5}=c^{\{S\}\times 2}_{9}\gamma_5,\ \omega^{\{3\}}_{9,6}=c^{\{S\}\times 2}_{9}\gamma_6,\ \omega^{\{3\}}_{9,7}=c^{\{S\}\times 2}_{9}\gamma_7\\
\omega^{\{3\}}_{10,1} &= -\left(\omega^{\{3\}}_{10,5}+\omega^{\{3\}}_{10,6}+\omega^{\{3\}}_{10,7}\right),\ \omega^{\{3\}}_{10,5}=c^{\{S\}\times 2}_{10}\gamma_5,\ \omega^{\{3\}}_{10,6}=c^{\{S\}\times 2}_{10}\gamma_6,\ \omega^{\{3\}}_{10,7}=c^{\{S\}\times 2}_{10}\gamma_7\\
\omega^{\{3\}}_{11,1} &= -\left(\omega^{\{3\}}_{11,8}+\omega^{\{3\}}_{11,9}+\omega^{\{3\}}_{11,10}\right),\ \omega^{\{3\}}_{11,8}=\gamma_8,\ \omega^{\{3\}}_{11,9}=\gamma_9,\ \omega^{\{3\}}_{11,10}=\gamma_{10}
\end{aligned} \tag{D.6}$$

where

$$\begin{aligned}
\gamma_5 &= \frac{1}{c^{\{S\}}_5(c^{\{S\}}_5-c^{\{S\}}_6)(c^{\{S\}}_5-c^{\{S\}}_7)},\ \gamma_6=\frac{1}{c^{\{S\}}_6(c^{\{S\}}_6-c^{\{S\}}_5)(c^{\{S\}}_6-c^{\{S\}}_7)},\\
\gamma_7 &= \frac{1}{c^{\{S\}}_7(c^{\{S\}}_7-c^{\{S\}}_5)(c^{\{S\}}_7-c^{\{S\}}_6)},\ \gamma_8=\frac{1}{c^{\{S\}}_8(c^{\{S\}}_8-c^{\{S\}}_9)(c^{\{S\}}_8-c^{\{S\}}_{10})}\\
\gamma_9 &= \frac{1}{c^{\{S\}}_9(c^{\{S\}}_9-c^{\{S\}}_8)(c^{\{S\}}_9-c^{\{S\}}_{10})},\ \gamma_{10}=\frac{1}{c^{\{S\}}_{10}(c^{\{S\}}_{10}-c^{\{S\}}_8)(c^{\{S\}}_{10}-c^{\{S\}}_9)}
\end{aligned} \tag{D.7}$$

This method satisfies all available coupling conditions (up through fourth-order) and its base method satisfies all order conditions up through fifth-order when

$$c^{\{S\}}_9=\frac{12-15c^{\{S\}}_{10}-15c^{\{S\}}_8+20c^{\{S\}}_{10}c^{\{S\}}_8}{15-20c^{\{S\}}_{10}-20c^{\{S\}}_8+30c^{\{S\}}_{10}c^{\{S\}}_8}. \tag{D.8}$$

References

[1] U.M. Ascher, S.J. Ruuth, R.J. Spiteri, Implicit-explicit Runge-Kutta methods for time-dependent partial differential equations, Appl. Numer. Math. 25 (2–3) (1997) 151–167.
[2] G.J. Cooper, A. Sayfy, Additive methods for the numerical solution of ordinary differential equations, Math. Comp. 35 (152) (1980) 1159–1172.
[3] G.J. Cooper, A. Sayfy, Additive Runge-Kutta methods for stiff ordinary differential equations, Math. Comp. 40 (161) (1983) 207–218.
[4] C.A. Kennedy, M.H. Carpenter, Additive Runge–Kutta schemes for convection–diffusion–reaction equations, Appl. Numer. Math. 44 (1–2) (2003) 139–181, http://dx.doi.org/10.1016/s0168-9274(02)00138-1.
[5] C.A. Kennedy, M.H. Carpenter, Higher-order additive Runge–Kutta schemes for ordinary differential equations, Appl. Numer. Math. 136 (2019) 183–205, http://dx.doi.org/10.1016/j.apnum.2018.10.007.
[6] A. Sandu, M. Günther, A generalized-structure approach to additive Runge–Kutta methods, SIAM J. Numer. Anal. 53 (1) (2015) 17–42, http://dx.doi.org/10.1137/130943224.
[7] M. Hochbruck, A. Ostermann, Explicit exponential Runge–Kutta methods for semilinear parabolic problems, SIAM J. Numer. Anal. 43 (3) (2005) 1069–1090, http://dx.doi.org/10.1137/040611434.
[8] V.T. Luan, R. Chinomona, D.R. Reynolds, A new class of high-order methods for multirate differential equations, SIAM J. Sci. Comput. 42 (2) (2020) A1245–A1268, http://dx.doi.org/10.1137/19M125621X.
[9] V.T. Luan, R. Chinomona, D.R. Reynolds, Multirate exponential Rosenbrock methods, 2021, arXiv:2106.05385.
[10] V.T. Luan, A. Ostermann, Explicit exponential Runge–Kutta methods of high order for parabolic problems, J. Comput. Appl. Math. 256 (2014) 168–179, http://dx.doi.org/10.1016/j.cam.2013.07.027.
[11] V.T. Luan, A. Ostermann, Parallel exponential Rosenbrock methods, Comput. Math. Appl. 71 (5) (2016) 1137–1150, http://dx.doi.org/10.1016/j.camwa.2016.01.020.
[12] M. Günther, A. Sandu, Multirate generalized additive Runge Kutta methods, Numer. Math. 133 (3) (2016) 497–524, http://dx.doi.org/10.1007/s00211-015-0756-z.
[13] A. Sandu, A class of multirate infinitesimal GARK methods, SIAM J. Numer. Anal. 57 (5) (2019) 2300–2327, http://dx.doi.org/10.1137/18M1205492.
[14] A. Sarshar, S. Roberts, A. Sandu, Design of high-order decoupled multirate GARK schemes, SIAM J. Sci. Comput. 41 (2) (2019) A816–A847, http://dx.doi.org/10.1137/18M1182875.
[15] J. Wensch, O. Knoth, A. Galant, Multirate infinitesimal step methods for atmospheric flow simulation, BIT Numer. Math. 49 (2) (2009) 449–473.
[16] R. Chinomona, D.R. Reynolds, Implicit-explicit multirate infinitesimal GARK methods, SIAM J. Sci. Comput. 43 (5) (2021) A3082–A3113, http://dx.doi.org/10.1137/20M1354349.
[17] D. Estep, V. Ginting, D. Ropp, J.N. Shadid, S. Tavener, An a posteriori–a priori analysis of multiscale operator splitting, SIAM J. Numer. Anal. 46 (3) (2008) 1116–1146, http://dx.doi.org/10.1137/07068237x.
[18] D.L. Ropp, J.N. Shadid, Stability of operator splitting methods for systems with indefinite operators: reaction-diffusion systems, J. Comput. Phys. 203 (2) (2005) 449–466, http://dx.doi.org/10.1016/j.jcp.2004.09.004.
[19] G.I. Marchuk, Some application of splitting-up methods to the solution of mathematical physics problems, Apl. Mat. 13 (2) (1968) 103–132.
[20] G. Strang, On the construction and comparison of difference schemes, SIAM J. Numer. Anal. 5 (3) (1968) 506–517, http://dx.doi.org/10.1137/0705041.
[21] R.J. Spiteri, S. Wei, Fractional-step Runge–Kutta methods: Representation and linear stability analysis, J. Comput. Phys. 476 (2023) 111900, http://dx.doi.org/10.1016/j.jcp.2022.111900.
[22] D. Goldman, T.J. Kaper, Nth-order operator splitting schemes and nonreversible systems, SIAM J. Numer. Anal. 33 (1) (1996) 349–367, http://dx.doi.org/10.1137/0733018.
[23] M. Calvo, J. De Frutos, J. Novo, Linearly implicit Runge–Kutta methods for advection–reaction–diffusion equations, Appl. Numer. Math. 37 (4) (2001) 535–549.
[24] C.A. Kennedy, M.H. Carpenter, Diagonally implicit Runge–Kutta methods for stiff ODEs, Appl. Numer. Math. 146 (2019) 221–244, http://dx.doi.org/10.1016/j.apnum.2019.07.008.

[25] S. Roberts, J. Loffeld, A. Sarshar, C.S. Woodward, A. Sandu, Implicit multirate GARK methods, J. Sci. Comput. 87 (1) (2021) 1–32.
[26] S. Roberts, A. Sarshar, A. Sandu, Coupled multirate infinitesimal GARK schemes for stiff systems with multiple time scales, SIAM J. Sci. Comput. 42 (3) (2020) A1609–A1638.
[27] A.N. Langville, W.J. Stewart, The Kronecker product and stochastic automata networks, J. Comput. Appl. Math. 167 (2) (2004) 429–447, http://dx.doi.org/10.1016/j.cam.2003.10.010.
[28] W.R. Inc., Mathematica, Version 13.2, Champaign, IL, 2022, URL https://www.wolfram.com/mathematica.
[29] P. Prince, J. Dormand, High order embedded Runge-Kutta formulae, J. Comput. Appl. Math. 7 (1) (1981) 67–75, http://dx.doi.org/10.1016/0771-050X(81)90010-3.
[30] C. Sanderson, R. Curtin, Armadillo: a template-based C++ library for linear algebra, J. Open Source Softw. 1 (2) (2016) 26, http://dx.doi.org/10.21105/joss.00026.
[31] C. Sanderson, R. Curtin, A user-friendly hybrid sparse matrix class in C++, in: J.H. Davenport, M. Kauers, G. Labahn, J. Urban (Eds.), Mathematical Software – ICMS 2018, Springer International Publishing, Cham, 2018, pp. 422–430.
[32] P. Bogacki, L. Shampine, A 3(2) pair of Runge–Kutta formulas, Appl. Math. Lett. 2 (4) (1989) 321–325, http://dx.doi.org/10.1016/0893-9659(89)90079-7.
[33] E. Hairer, G. Wanner, Solving Ordinary Differential Equations II. Stiff and Differential-Algebraic Problems, Vol. 14, Springer, 1996.
[34] A.C. Fish, D.R. Reynolds, Adaptive time step control for multirate infinitesimal methods, SIAM J. Sci. Comput. 45 (2) (2023) A958–A984, http://dx.doi.org/10.1137/22M1479798.